

Article

Wind Resource Assessment in Building Environment: Benchmarking of Numerical Approaches and Validation with Wind Tunnel Data

Costa Paula ¹, Cataldo José ², Mazaira Leorlen ^{3,4}, González Daniel ^{3,4} , Costa Alexandre ^{3,5} and Simões Teresa ^{1,*}

¹ National Laboratory for Energy and Geology (LNEG), 2610-999 Lisbon, Portugal

² Instituto de Mecánica de los Fluidos e Ingeniería Ambiental (FING-UDELAR), Montevideo 11300, Uruguay

³ Center for Renewable Energy, Federal University of Pernambuco (CER-UFPE), Recife 50670-901, Brazil

⁴ Graduate Program in Nuclear and Energy Technologies (PROTEN), Federal University of Pernambuco (UFPE), Recife 50670-901, Brazil

⁵ Department of Nuclear Energy (DEN), Federal University of Pernambuco (UFPE), Recife 50670-901, Brazil

* Correspondence: teresa.simo@lneg.pt; Tel.: +351-210924775

Abstract: In the framework of the wind energy network for distributed generation in urban environments for most South American countries, wind resource assessment studies have been carried out in activities to establish a suitable methodology to assess the wind potential in urban environments. Some methodologies are already published in research studies, and the wind tunnel is the most accurate solution to obtain insight into the wind resource when measurements are unavailable, which is the most frequent case. Nevertheless, besides its validity, one cannot disregard the high cost of producing a scaled urban model and access to a wind tunnel. In this sense, this paper compares results from a wind tunnel experiment and different numerical modeling approaches. Two commercial models (WindSim and Wasp Engineering) and one open-source CFD code (OpenFOAM) are used. The results from the modeling simulation concluded that CFD models could achieve lower deviations for the mean wind speed and turbulence intensity when compared with non-CFD models. With such results, CFD modeling is a promising tool for reliably evaluating wind potential in urban environments.

Keywords: wind resource assessment; building environment; numerical modeling; CFD; wind tunnel simulations; urban area; wind flow



Citation: Paula, C.; José, C.; Leorlen, M.; Daniel, G.; Alexandre, C.; Teresa, S. Wind Resource Assessment in Building Environment: Benchmarking of Numerical Approaches and Validation with Wind Tunnel Data. *Wind* **2022**, *2*, 659–690. <https://doi.org/10.3390/wind2040035>

Academic Editor: Yasushi Uematsu

Received: 12 August 2022

Accepted: 21 October 2022

Published: 27 October 2022

Publisher's Note: MDPI stays neutral with regard to jurisdictional claims in published maps and institutional affiliations.



Copyright: © 2022 by the authors. Licensee MDPI, Basel, Switzerland. This article is an open access article distributed under the terms and conditions of the Creative Commons Attribution (CC BY) license (<https://creativecommons.org/licenses/by/4.0/>).

1. Introduction

In recent years, several governments have made efforts to define measures to mitigate climate change effects and reduce greenhouse emissions (GHE). These measures were established in Europe by the publication of national climate and energy plans and outside Europe through similar programs, such as National Energy Plans 2030 and 2050 for Brazil. In this context, the installation of renewable energy systems has been incentivized, not only through large power centrals but also through distributed generation by installing small renewable energy systems. In this sense, urban wind assumes a relevant role in the contribution to the accomplishment of the national goals on energy and climate.

The wind potential in urban areas and the use of small wind energy systems have become very popular [1–3] in recent years, especially in the context of smart and sustainable cities. In addition, the costs associated with the installation of these systems are low when compared to wind farms.

However, the wind in urban environments is very complex due to the presence of buildings and urban elements, making the wind very unpredictable and contributing to the existence of high turbulence [4–6]. The spatial variability of the wind flow is especially relevant in urban contexts, where the wind speed varies drastically over short distances [4,6]. Specific approaches for wind resource assessment in an urban environment have been proposed [6,7] and are of major importance, especially when there are very little or even

non-observational data [8,9]. However, there are still challenges in predicting the wind flow over specific areas inside the urban area, particularly between tight streets and dense and irregular buildings [10–12].

In what concerns wind measurements in an urban environment, these are frequently conducted using ultrasound anemometry rather than the conventional cup devices since, desirably, the characterization of the 3D wind is needed. In recent years, some experiments have been conducted using LiDAR (Light Detection and Ranging) measurement systems by the scientific community for this purpose, according to Refs. [2,13–15], used mainly in the scope of R&D projects due to the high investment associated with the acquisition and maintenance of this type of equipment.

Moreover, the accuracy of the urban fabric represents a challenge in the modeling of the urban wind resource [16,17]. Although several municipalities already have accurate representations of the cities' urban fabric, they are not easily accessible to most users. Solutions related to the use of airborne LiDARs are available but with remarkable costs. Therefore, most studies are conducted in small areas within a city representing small groups of buildings or neighborhoods. The use of satellite images or Ortho-photomaps, geographical information techniques and manual digitalization of the buildings (using GIS—Geographical Information System) may be used to obtain the urban fabric, although the accuracy may be reduced. However, some research databases enable us to obtain the urban fabric in some cities and use it in resource assessment models. An example is the NUDAPT database project (National Urban Database with Access Portal Tool), which enables the downloading of 2D and 3D building information for some American cities (<http://www.nudapt.org>, accessed on 27 July 2022).

The most suitable models to use in the study of urban wind are CFD based (Computational Fluid Dynamics). Such models have proved through the years to present valid results in small areas, such as small groups of buildings and isolated buildings. The same is not entirely true when one wishes to perform the wind resource assessment in larger areas. In this case, these models can be very time-consuming. In addition, the use of CFD standard codes is not user-friendly and demands, in most cases, a deep knowledge of the fluid mechanics processes involved and, most of the time, advanced programming skills. In addition, most of the available models have expensive commercial licenses since they are dedicated to a large set of research topics. Nevertheless, freeware models are also available, although their use is frequently less user-friendly. An example of a freeware CFD code is OpenFOAM, whose capabilities have been widely used in urban wind applications, according to Refs. [18–21].

In recent decades, several models that can be used for this objective have been developed and, with special care on the input data (data series and urban fabric), enable us to obtain good results. Examples are WindSim (<https://www.windsim.com>, accessed on 27 July 2022) and OpenFOAM (see Section 3 for more detail).

Finally, the physical modeling of the wind behavior in a wind tunnel is one of the most accurate solutions to obtaining the wind flow in urban areas when measurements are unavailable [6,7]. Nevertheless, besides its validity, one cannot disregard the high costs associated with the scaled urban model and the access to the wind tunnel.

Therefore, this paper takes the wind tunnel simulation as the baseline for benchmarking two specific commercial CFD-based tools (WASP Engineering and WindSim) and a general-purpose open-source CFD code (OpenFOAM) to evaluate the wind flow over a complex urban area and makes some considerations about the applicability of each model in simulating the wind flow over areas of the city that the actual literature [12,16,17] still appoints as challenging areas to predict the wind behavior inside an urban area.

2. The Wind in the Urban Environment

The atmospheric boundary layer (or planetary boundary layer) is the portion of the atmosphere closest to the earth's surface. In this planetary boundary layer, several sublayers are identified according to [22,23] such as in Figure 1. In the wake and logarithmic sub-

layers, an analytical model can describe the mean velocity profile. At the same time, the roughness sub-layer is a non-homogeneous flow region imposing changes to the vertical velocity profile. When the wind blows over a city, inside the roughness sub-layer, the flow occurs in an urban environment composed of multi-block low-rise and high-rise buildings and squares, trees, and shorelines.

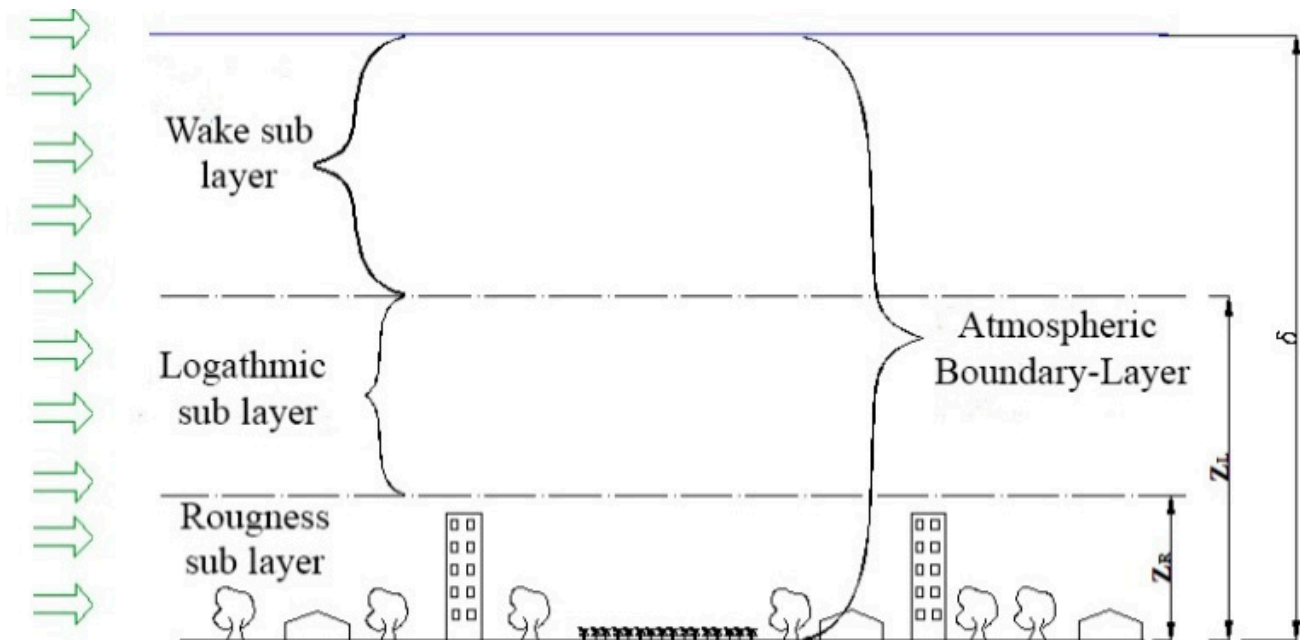


Figure 1. Atmospheric boundary layer sublayers.

Since wind in urban areas is strongly three-dimensional, the aerodynamics of the buildings must be studied in detail. The wind around buildings and its aerodynamic effects have been previously studied by Refs. [10,24,25]. They give examples of flow behavior around buildings in different situations and the loads associated with such interactions. Several of these cases have been included in codes such as ASCE (2017) [26] and EUROCODE (2007) [27]. When analyzing the wind flow around a bluff body in an isolated condition, it is possible to verify several three-dimensional effects experimentally; some of these are depicted in Figure 2.

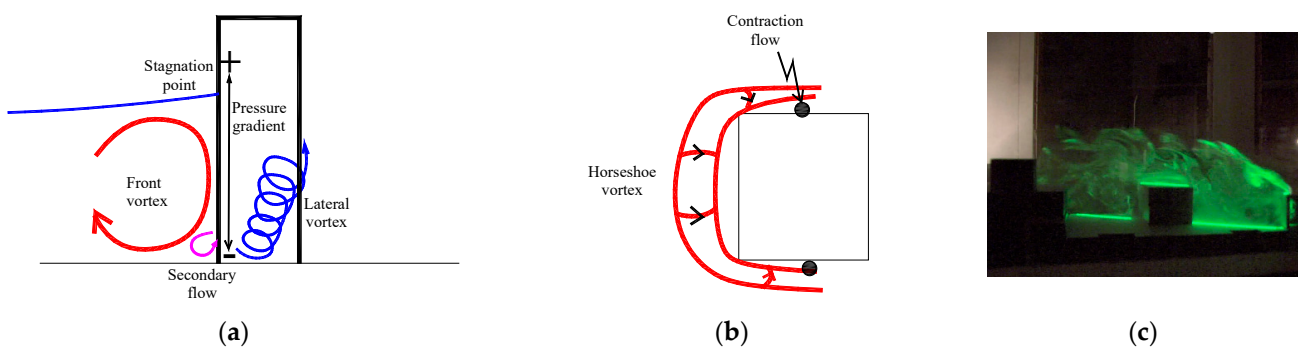


Figure 2. Typical flows around bluff bodies: (a) the common boundary layer separation with the production of vortices and turbulence; (b) the common horse-shaped vortices developed at the base of high buildings developing strong convergence/divergence of the flow producing strong vorticity gradients; (c) the flow complexity around multiple obstacles very closed to each other as seen by a wind tunnel experiment.

Because of wind flow and the building interaction, a pressure field is generated on the building envelope. Boundary layer separation, velocity gradient, vorticity, and turbulence

production, occur around the building (Figure 2a). Recirculation and accelerated flow regions appear, and vortex emissions can occur. The extension of the different regions depends on building geometry. For example, if the building is longer than the height, the flow is reattached, and the recirculation region downstream is similar to the building height. If the building is shorter, the separation region increases [28].

For high-rise buildings, a horseshoe-shaped vortex develops at the base of the building and a strong pressure gradient is established on the front face (Figure 2b). In addition, very high velocities occur near the ground. In addition, and beyond the vortex's zones, the separation effects induced by buildings with irregular shapes cause a wind speed deficit and excess turbulence in the boundary region of each building, extending the dimensions of each vortex up to 5 to 20 building heights downstream [28]. However, in most urban areas, the buildings are close to each other, originating a complex interaction between flow and obstacles since the flow does not return to the initial condition (Figure 2c).

In a conceptual form, the urban area configuration will influence the wind flow behavior producing three different types of flow regimes—isolated, interference, and skimming [29]. An isolated flow is when the urban elements are far apart and let the wind flow act like an individual wake generator at the urban elements. The interference flow is when the urban elements are very close and make wakes reinforce each other. The skimming flow is when the density of urban elements is so high that it makes the wind flow slip over the top of the urban elements [30].

In a city, different types of terrain can be identified [31]. There are uniform regions where the buildings have similar geometries. For example, “high-rise buildings surrounded by high-rise buildings” or “low-rise buildings surrounded by low-rise buildings”. There is also a boundary region where the geometry changes or the open-face regions are directly exposed to the wind from the sea or from rural areas [31]. Although the urban environment may have uniform regions, some differences between buildings' geometry can force the wind flow to behave as a stagnation zone over the building or develop strong turbulence or a chain of trailing vortices between tall trees.

In summary, in certain conditions, such as a significant height above the ground, the flow could be analytically well modeled, but still, a physical or numerical modeling technique must be used in the roughness sub-layer to describe the three-dimensional flow behavior.

3. Methodology and Models

The methodology developed for this work is based on three main steps. The first consists of an experiment over an urban area modeled in a wind tunnel. The second of the numerical modeling of the wind flow using three different tools, and the third of validating the numerical modeling results based on a wind tunnel experiment.

The tools used are: WAsP Engineering [32], a simplified physical model to describe the wind flow over complex terrain and close to sheltering obstacles [30], WindSim [33], a CFD commercial tool for complex terrains and wind flow over wind farms [31], and OpenFOAM [34], a free general purpose open source CFD code able to describe the wind flow around obstacles [32]. The three models have different scopes of use, but in a general way, they can show reliable results for wind behavior in urban environments.

3.1. Wind Tunnel

The Wind tunnel is an open section type with a test section of 17 m long, 2.25 m wide, and 2.1 m high, which is illustrated in Figure 3a and is installed in the School of Engineering of the Universidad de la República in Uruguay. The wind tunnel can provide a constant wind flow or a well-defined wind profile if coupled with an artificial Standen method [35,36] (Figure 3b) which can reproduce any vertical wind profile according to the desired roughness and mean wind speed for the free atmosphere, keeping the temperature and atmospheric pressure constant during the experiment.

The wind tunnel was configured to provide the vertical wind speed profile for the area outside the surroundings of the urban area, where the roughness height is classified

as 1 m, and the wind speed is 13 m/s at 90 m. To describe these conditions, the Standen method coupled with the wind tunnel is formed with three spires of 1.2 m high, a barrier of 30 cm high, and a rough floor of 12.8 m long composed of cubes 30 mm side located in scatter. The distance between cube lines is 9.3 cm, and the distance between cubes in a line is 18.6 cm. This method aims to inquire about the vertical wind speed profile and turbulence properties in the approximation region of the urban area. This analysis was developed considering the methodology described in Ref. [37].

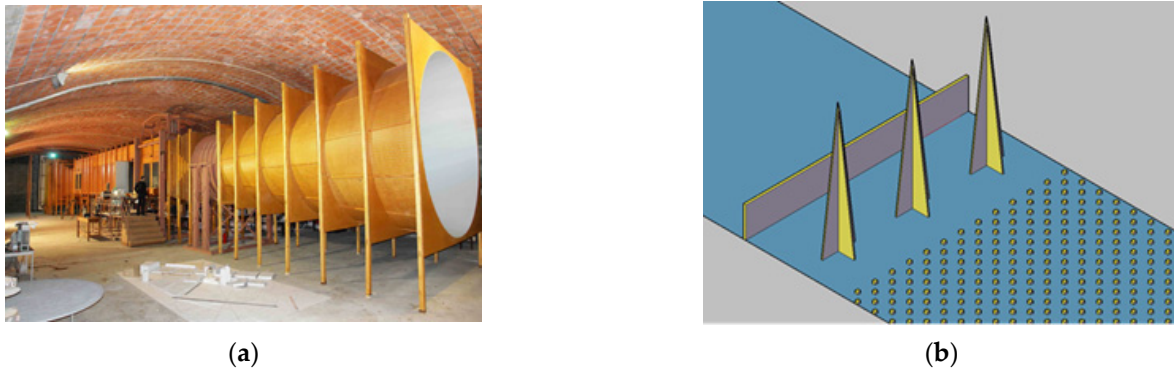


Figure 3. (a) Wind tunnel at the School of Engineering of the Universidad de “la República” Uruguay; (b) the Standen Method for the establishment of the vertical wind profile according to roughness length and mean wind speed.

The urban area and the approximation region were modeled at a geometrical scale of 1/100. Figure 4a shows the model, including the urban area highlighted in purple and the surrounding in grey. Figure 4b shows the IFA 300 hot wire/film anemometer of three channels under operation, which can measure the three components of the wind flow. Data acquisition was performed with a National Instruments A/D card and a programming code to read the data developed in CVI Lab Windows. The IFA 300 hot wire/film is mounted in a four-freedom degree positioner system, as shown in Figure 4b. The central urban area—in purple—is prepared to rotate 360° degrees to model the wind flow effect from any angle.



Figure 4. (a) Urban area and surroundings model at a geometrical scale of 1/100. The purple area represents the focus urban area to be evaluated by numerical models; (b) the IFA 300 hot wire/film under operation mounted in a four-degree positioner.

3.2. Windsim Model

This model was developed specifically for wind energy applications in complex terrains, assuming, as inputs, wind data series, orography and roughness description, and obstacles, and it uses a structured and Cartesian mesh. Figure 5 illustrates a simplified scheme with the workflow of the model.

This model solves the Reynolds Average Navier–Stokes equations for the mean flow (RANS) with the finite element method, starting with solution estimates as initial conditions. The evolution of the model’s convergence may be visualized at a selected point, as well as the values of the flow parameters and the residuals of the numerical simulation. The resolved variables are the pressure, the three wind speed components (u , v , and w), the turbulent kinetic energy, and the turbulent kinetic energy dissipation rate. It has two types of solvers, segregated and coupled. One of the disadvantages of the first solver is the difficulty of convergence when modeling a large number of cells. Coupled (MIGAL) [38] uses the coupling technique—velocity–pressure and a linear solver that simultaneously updates the velocity and pressure fields in the entire domain. Since this is an algebraic linear solver, it only executes the first part of the velocity–pressure iteration. After this process, the PHOENiCS model completes the non-linear part of the iteration (<http://www.cham.co.uk>, accessed on 27 July 2022). In terms of convergence, this solver converges with much fewer iterations, despite requiring greater storage capacity than the previous one. The process adopted by this model involves the execution of several modules whose included models are operated in a chained way until the results are obtained.

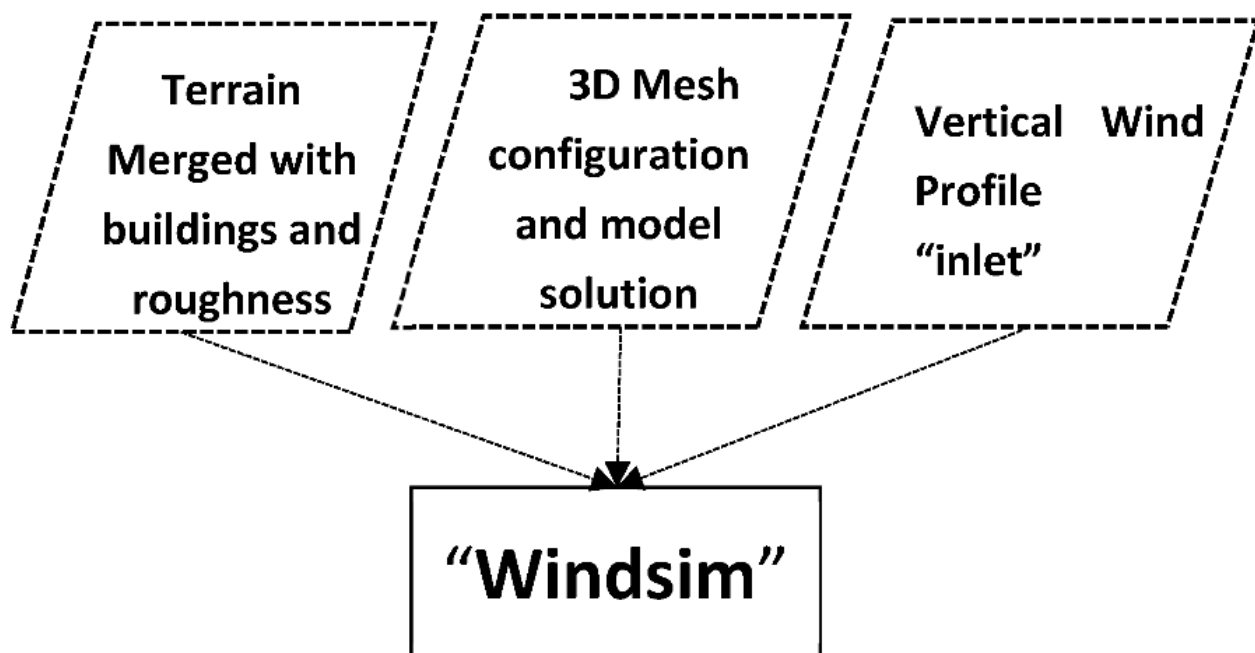


Figure 5. Schematic workflow for performing a simulation with the WindSim model.

3.3. WAsP Engineering Model

WAsP Engineering is the industry-standard modeling software to calculate wind conditions over complex terrain and around wind farms. This model is fed with initial conditions, such as an urban digital terrain model, equivalent characteristic roughness value in the simulation area, and vertical wind profile parameters. Figure 6 depicts a schematic workflow of the model.

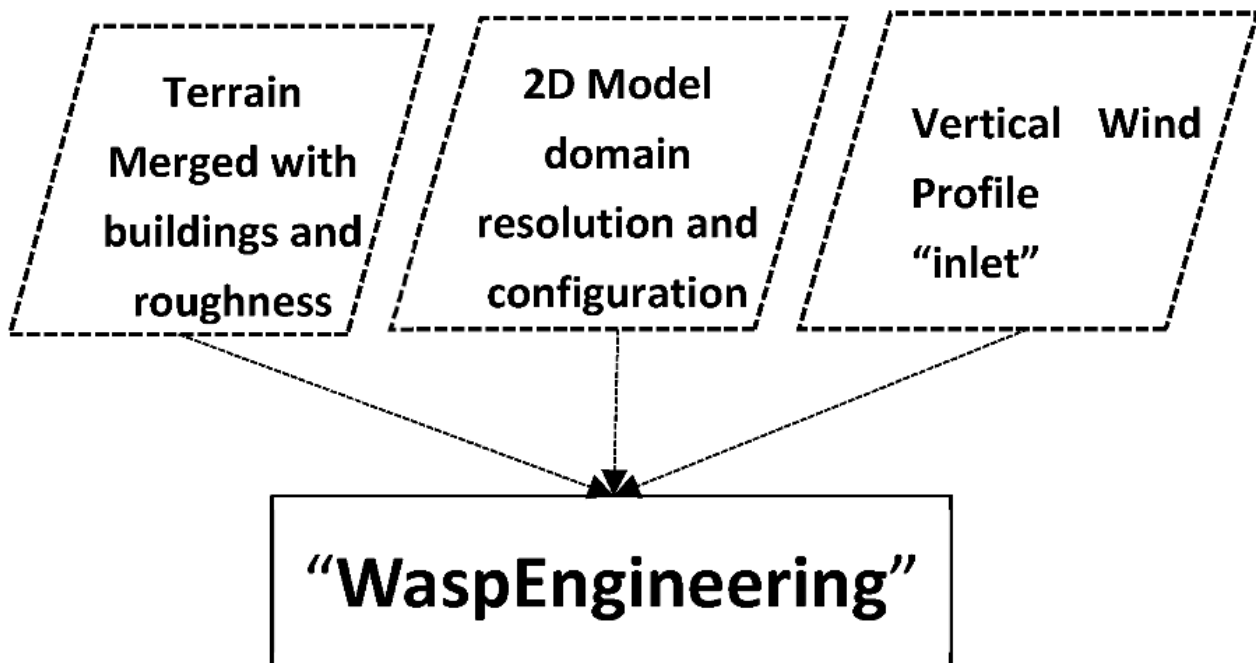


Figure 6. Schematic workflow for performing a simulation with WASP Engineering.

The model solves the wind flow for stationary situations through the linear solver LINCOM [32]. This solver does not depend on time steps since it is neither iterative nor convergent. The model has a set of simplified parametrizations for atmospheric turbulence and solves the adiabatic effects of the mountain areas and recirculation zones in complex terrains and wake-effect models adapted according to the type of wind turbine and soil roughness. It also has a simplified scheme to deal with the thermal stratification of the atmosphere.

3.4. OpenFOAM Model

OpenFOAM is a free, open-source CFD code based on numerical routines to process the input information to the CFD model and routines for post-processing the results. It is efficient, easily adaptable and flexible. OpenFOAM's SnappyHexMesh utility was used to snap the grid around the imported Stereolithography (STL) file with the geometry of interest. In this work, we used the version OpenFOAM-v2012 (<https://www.OpenFOAM.com>, accessed on 27 July 2022), released on 23 December 2020, adopted with the steady-RANS, $k-\varepsilon$ turbulence model. This model is an appropriate choice for wind CFD modeling in complex terrains and urban wind applications [39].

Figure 7 shows a simplified view of the numerical routines applied in this work (in operation order) and the type of information addressed for the full operation of each numerical module.

The OpenFOAM solver SimpleFoam is based on the SIMPLE algorithm (Semi Implicit Method for Pressure Linked Equations) [40], which solves the single-phase, incompressible, and steady-state Navier–Stokes equations.

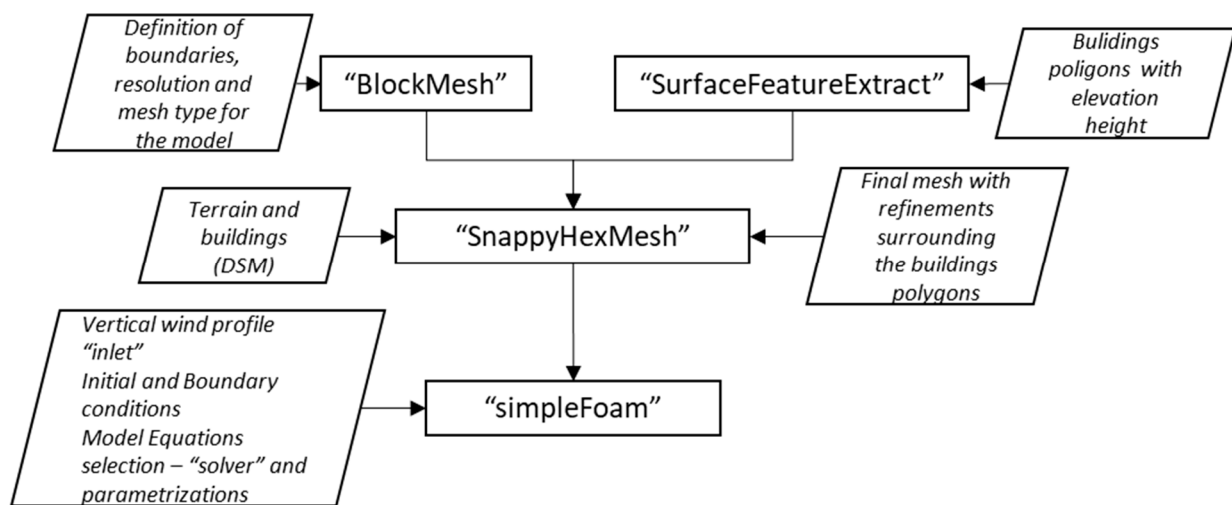


Figure 7. Schematic workflow for performing a simulation with the OpenFOAM model.

4. Case Study

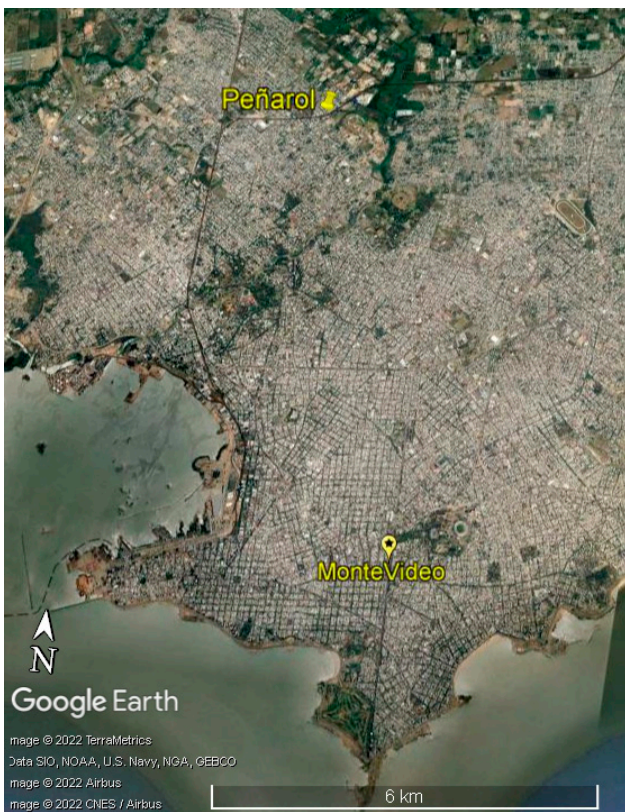
The selected case study is Peñarol, an urban area in Montevideo (Uruguay). Figure 8a shows the area under study in Google Earth, where Montevideo is illustrated with emphasis on the Peñarol neighborhood and the Carrasco International Airport. Figure 8b illustrates a zoomed view of the urban area under analysis. Most of the constructions are houses or buildings, with dense distribution and with heights varying between 3 m to 6 m. The area is characterized by narrow roads, which makes it a challenging zone for urban wind resource assessment.

In the Peñarol area, no experimental data enable us to characterize the wind flow and turbulence. The closest meteorological mast is located at the International Airport of Carrasco, 10 km east of Peñarol. The measured data corresponds to ten years of hourly wind and direction observations, obtained at 10 m height and enabled us to provide a preliminary estimate of the wind speed and direction at measurement height. Using analytical modeling techniques [41], it was possible to evaluate the wind flow (speed and direction) at 90 m height for a flat area outside the surroundings of the urban area with a roughness height classified as 1.0 m [28]. The wind tunnel experiment was configured to provide a reliable vertical wind profile following the results. For this case, the wind speed reaches approx. 13 m/s at 90 m height.

4.1. Wind Tunnel

With the help of the IFA 300 hot wire/film anemometer, several reads of the three wind components at different heights (up to a scale of 90 m height) were obtained for the surrounding urban area (a grey area near the purple area—see Figure 4a) to provide a reliable vertical wind profile and turbulence intensity inlet conditions for CFD modeling. The surrounding urban area covers a circular area with a radius of 200 m around the central point of the urban area. The results obtained for the grey area are depicted in Figure 9a,b, which represent the vertical wind profile read probes and the adjusted logarithmic vertical wind profile, and the turbulence intensity results, respectively.

The wind tunnel results show a vertical wind speed profile with a maximum mean wind speed of 12.95 m/s reached at 60 m height above ground level with a converged turbulence intensity of 18%. With these wind tunnel results, it was also possible to derive a sub-urban flow correspondent to the Peñarol neighborhood (Figure 9a) and a computed roughness length of 0.87 m obtained from the adjustment of a logarithmic law to the data. These results constitute the inlet conditions for the numerical models under evaluation.

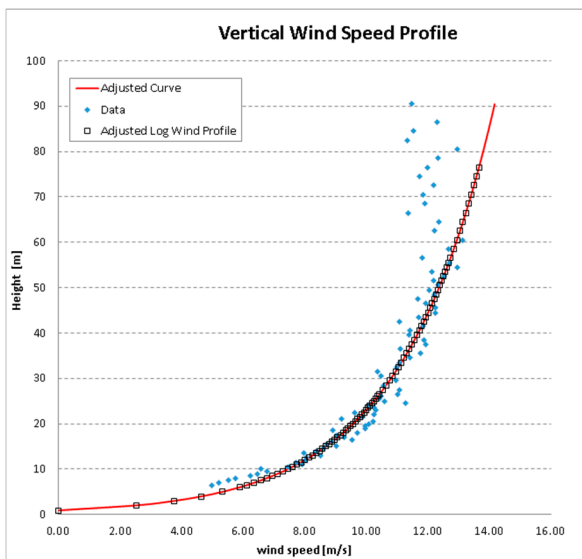


(a)

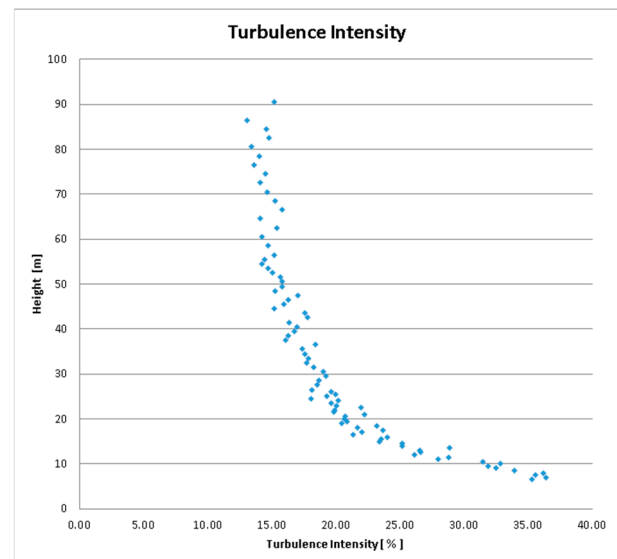


(b)

Figure 8. (a) Montevideo City with the location of the urban area under study merged in the surroundings of the Peñarol area; (b) zoom overused area for the case study.



(a)



(b)

Figure 9. (a) Estimated vertical wind profile at the surrounding urban area; (b) the turbulence intensity distribution by several reads at different heights up to scaled 90 m height.

To validate the performance and results of the models WindSim, OpenFOAM, and WAsP Engineering, when compared with the Wind Tunnel data, a set of 11 sites inside the urban area were established (Figure 10a). For each of the 11 sites, three measures of

the wind flow were collected at 3 m, 7 m, and 15 m high above the buildings' rooftops, representing approximately 6 m, 12 m and 17 m above the ground. All measures were taken with the help of the IFA 300 hot wire/film, as previously described. Measures were taken at 22.5° degree intervals (referenced in the meteorological North, see Figure 10b), corresponding to 16-degree sectors (N, NNE, NE, ENE, E, ESE, SE, SSE, S, SSW, SW, WSW, W, WNW, NW, and NNW). However, to decrease computational costs related to the various numerical experiments, only the results for sectors that are multiples of 45 degrees will be presented hereafter.

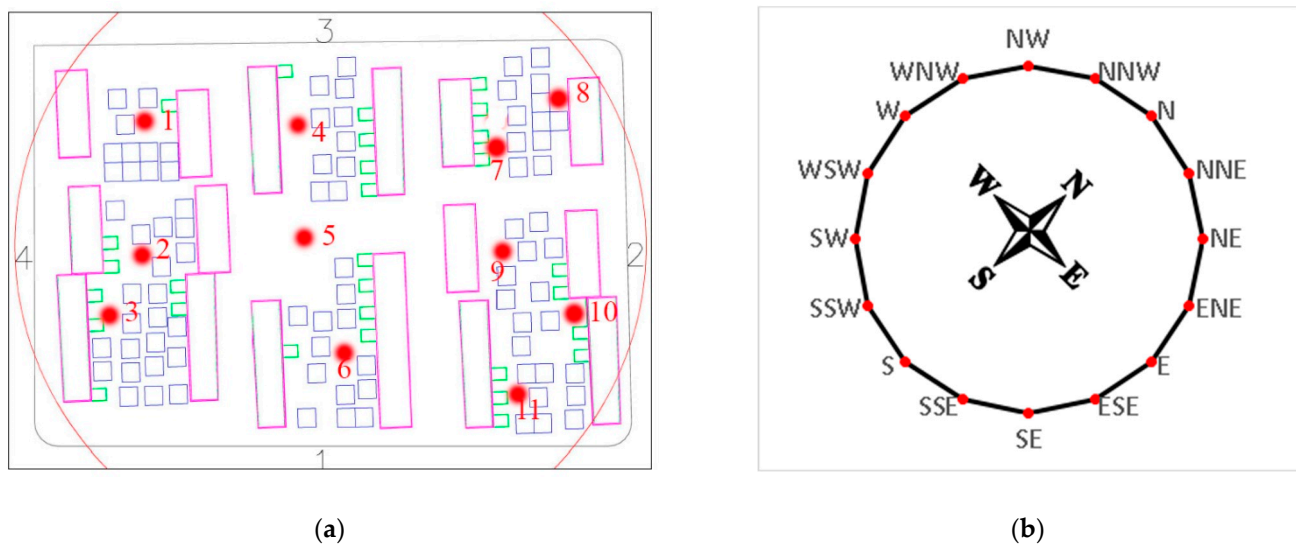


Figure 10. (a) Location of the 11 probe points in the wind tunnel to infer the wind flow at three different heights above ground level; (b) Sixteen-degree rotating sectors (according to wind rose) for probing the data according to the projection of (a).

4.2. Geometry and Domain Simulations

To represent the urban area and its surroundings, a prototype scaled at the 1/100 model was created. The model includes the area of interest and its surroundings, forming a circular area with a 200 m radius (from the central point of the area under study, red rectangle in Figure 11). The circular model of the urban area is depicted in Figure 11.

Due to its nature, WASP Engineering and WindSim models cannot directly use a mesh exclusively formed with buildings since they are mostly dedicated to wind farm resource assessment. In this sense, there was the need to include the terrain. Therefore, an STRM–30m [42] terrain for the Peñarol area was extracted, and, using the method in Simões and Estanqueiro (2016) [3], it was possible to build a digital urban terrain model of the area (Figure 12a). The heights of the buildings are represented in Figure 12b.

The following phase was the creation of a mesh suitable for both models, WASP Engineering and WindSim. The WASP Engineering model can only be configured with regular meshes. Therefore, a mesh of 0.5 m × 0.5 m was created and is depicted in Figure 13a. For the case of the WindSim model, one can configure regular or irregular mesh plus a nested grid. For this experiment setup, an irregular mother domain mesh of 4 m × 4 m was created and merged with an irregular nested mesh with 2 m × 2 m spatial resolution, covering the central part of the urban area—Figure 13b.

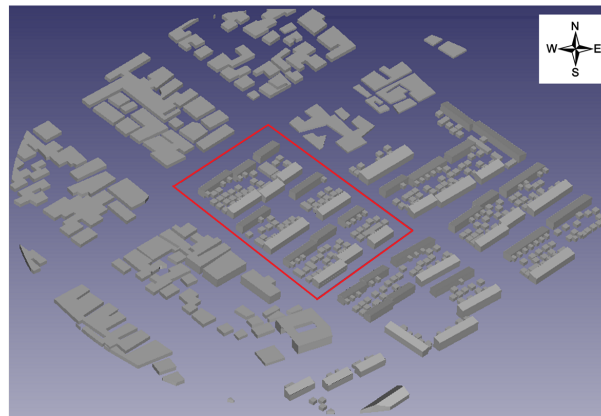


Figure 11. Circular urban area model (red area—the focus urban area) with surroundings at a scale of 1/100 with a radius of 200 m from the midway point.

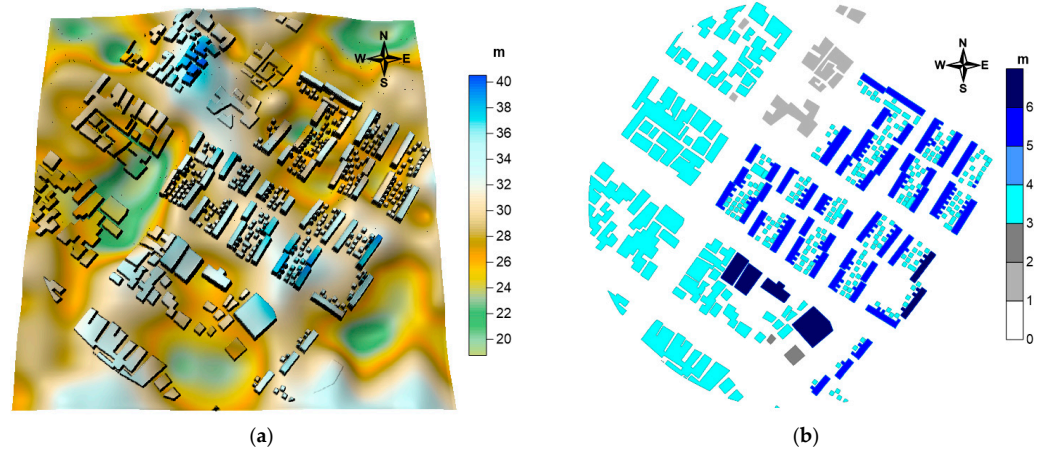


Figure 12. (a)—Digital urban terrain model of the urban area for WASP Engineering and WindSim models—Vertical exaggeration of 1.5×; (b) Buildings height.

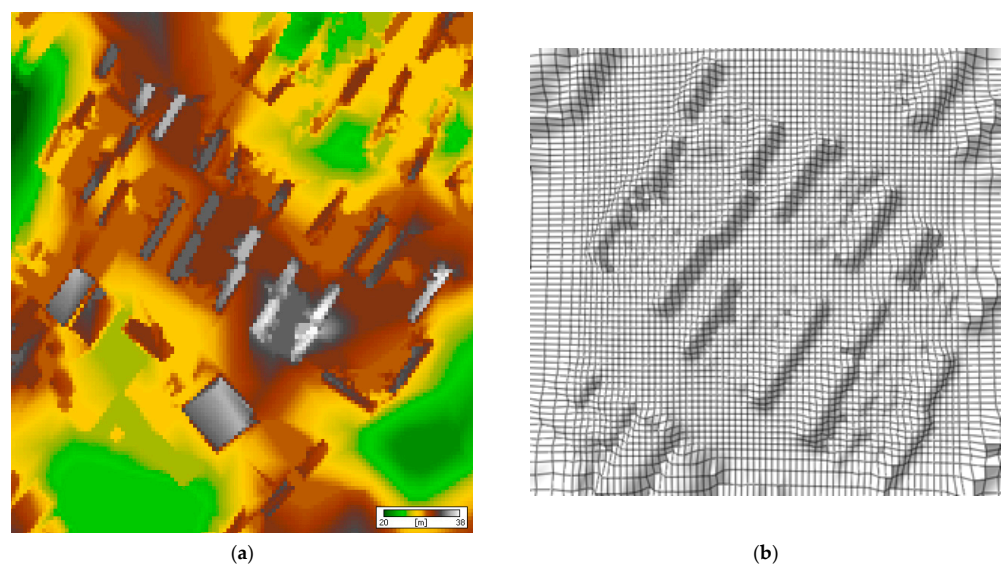


Figure 13. (a)—Digital urban terrain model at 0.5 m × 0.5 m spatial resolution computed by WASP Engineering; (b) Regular nested mesh generated by WindSim model for the central urban area with 2 m × 2 m spatial resolution.

In terms of the vertical structure of the mesh, the WASP Engineering model solves the Lincon model for a 2D XY user-defined horizontal level above ground level. Nine horizontal X-Y section plans were established at 9 m, 12 m, 17 m, 30 m, 40 m, 60 m, 90 m, 120 m, and 200 m above ground level. The urban area's results and surroundings are based on the lowest three levels (9 m, 12 m, and 17 m). The level at 200 m height was defined to inquire about the free atmospheric wind flow at the top of the boundary layer.

The WindSim model can be configured with a 3D vertical structure with or without a nested refined mesh. For the urban area and its surroundings, a 3D mesh with eight levels was defined, imposing eight vertical levels for the grid, namely at 1 m, 17 m, 62 m, 135 m, 238 m, 369 m, 529 m, and 717 m to keep model convergence stable for all angles. Figure 14 shows a partial extract of the vertical structure of the refined mesh generated by the WindSim model.

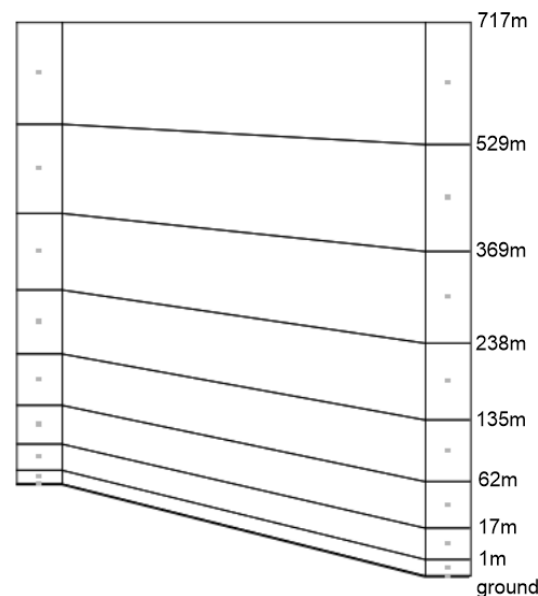


Figure 14. Schematic representation of the 3D vertical structure refined mesh generated by WindSim model. Eight vertical levels were considered to meet the convergence criteria of the CFD solver.

In OpenFOAM, an STL file with the geometry of the urban area of interest was created for the generation of the computational domain geometry. Using the SnappyHexMesh tool. The whole domain consists of a box, which was rotated to be aligned with the inlet direction. The mesh comprises hexahedral elements and contains two zones, a circular subdomain to frame the building's zone and another for the rest of the domain. The circular area was refined (buildings area) in order to detail and better characterize the building's zone where the largest velocity and pressure gradients will occur. The k- ϵ standard model was adopted as the turbulence closure model.

Figure 15 shows the mesh used for the computational domain.

A mesh independence study with an imposed hypothetical vertical wind profile was performed to guarantee the independence of the results with the size of the adopted elements (see Figure 16). To do this, a simulation was performed with three different meshes, reducing the size of the elements of both regions. Mesh 1 has 22.9 million cells, Mesh 2 has 18.2 million cells, and Mesh 3 has 25.4 million cells. Values of velocity were taken at probe points per height and compared with results obtained from the wind tunnel adapted to the hypothetical vertical wind profile. Mesh 1 is used in OpenFOAM, considering the calculation accuracy and convergence velocity presenting slightly fewer deviations than Meshes 2 and 3.

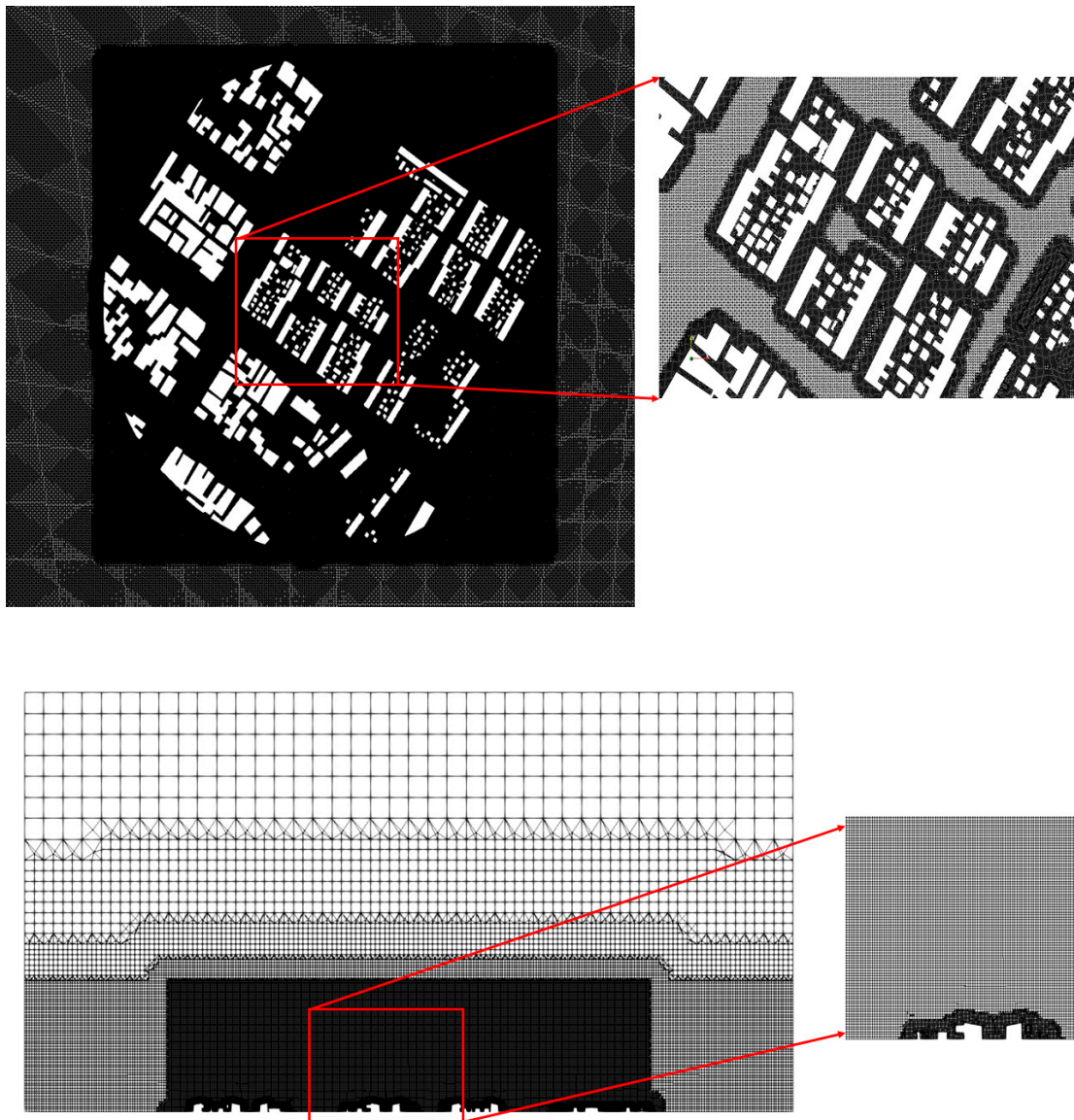


Figure 15. Mesh used for the OpenFOAM computational domain, detailing the zones used for different element sizes near the building’s walls.

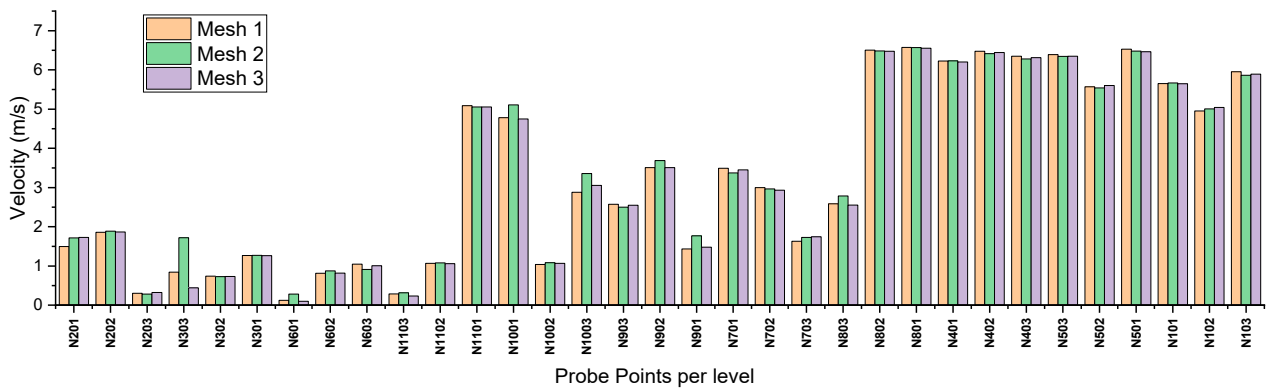


Figure 16. Mesh independence study considering three different meshes for the OpenFOAM computational domain. Velocity in validation points. Hypothetical vertical wind profile considered.

4.3. Initial and Boundary Conditions for Modeling Simulations

Table 1 shows the options imposed for the initial and boundary conditions for the simulations with WASP Engineering. Table 2 shows the options defined to meet the convergence criteria for Windsim. Finally, Table 3 shows the options and parameters defined for the simulations with OpenFOAM.

Table 1. Initial and boundary conditions imposed for the WASP Engineering model.

Model Version	WASP Engineering v. 2.0
Initial Conditions	<ul style="list-style-type: none"> • Urban digital terrain model • Top of boundary layer: 200 m height above ground • Spatial resolution: 0.5 m × 0.5 m • Roughness length: $Z_0 = 0.87$ m (<i>dense occupation</i>);
Boundary Conditions	<ul style="list-style-type: none"> • Nonslip wall function (constant value of 0.03); • Vertical wind profile: <ol style="list-style-type: none"> a. $Z_{\text{ref}} = 60$ m b. $Z_0 = \text{uniform} = 0.87$ m (<i>dense occupation</i>) c. $Z_{\text{ground}} = 0$

Table 2. Initial and boundary conditions imposed for the Windsim model.

Model Version	Windsim v. 6.0
Initial Conditions	<ul style="list-style-type: none"> • Urban digital terrain model • Top of boundary layer: 800 m height above ground • Refined orthogonal 3D grid: 2 m × 2 m • Roughness Height: $Z_0 = 0.87$ m (<i>dense occupation</i>) • Height distribution factor: 0.01 • Ratio additive length to resolution: 0.01 • Smoothing Gaussian model: <ol style="list-style-type: none"> a. Terrain smoothing limit: 0.01 b. Smoothing radius: 0 c. Gradual smoothing type: Inner gradual smoothing
Boundary Conditions	<ul style="list-style-type: none"> • Low height for boundary layer: 200m • Speed at low height for boundary layer: 13 m/s • Top boundary condition: Fixed pressure • Vertical wind profile: <ol style="list-style-type: none"> a. $Z_{\text{ref}} = 60$ m b. $Z_0 = \text{uniform} = 0.87$ m (<i>dense occupation</i>) c. $Z_{\text{ground}} = 0$ d. Turbulence Intensity = 0.18
Calculation Parameters	<ul style="list-style-type: none"> • Solver: GCV • Number of iterations: 200 • Convergence criteria: 0.005 • Potential temperature: Disregard temperature • Air density: 1.225 kg/m³ • Turbulence model: modified k-ε • Height of reduced wind database: 200 m

Table 3. Initial and boundary conditions imposed for the OpenFOAM model.

Model Version	OpenFOAM v. 2012
Initial Conditions	<ul style="list-style-type: none"> • STL model of the urban area • Top of boundary layer: 300 m height above ground • Minimum grid size: 0.5m • Aerodynamic roughness length: $Z_0 = 0.087$ m
Boundary Conditions	<ul style="list-style-type: none"> • Speed above boundary layer height: 13 m/s • Top and sides boundaries: Slip • Inlet condition: atmBoundaryLayerInletVelocity <ol style="list-style-type: none"> a. $V_{ref} = 12.95$ m/s b. $Z_{ref} = 60$ m c. $Z_0 = \text{uniform} = 0.087$ m d. $Z_{ground} = 0$
Calculation Parameters	<ul style="list-style-type: none"> • Solver: simpleFoam • Number of iterations: 5000 • Convergence criteria: 0.0001 • Potential temperature: Disregard temperature • Air density: 1.225 kg/m³ • Turbulence model: standard k-ϵ

4.4. Results

4.4.1. Wind Tunnel Results

The wind tunnel measurements are presented in Table 4. Values are computed for the eight wind rose directions (45° sectors). The results presented are the relation between measured wind speed (V) and the defined wind speed at the top of the boundary layer (VH) and the turbulence intensity values (TI) expressed in percentage. Moreover, these results are presented for each test point, P.1, P.2, and P.3, where P is the point number (1 to 11), and 1,2,3 are the respective median heights above ground level, respectively, 9 m, 12 m, and 17 m.

Table 4. Wind tunnel results per direction per point (1 to 11) and per height. V/VH is the ratio between velocity (V) and velocity at the top of the boundary Layer (VH); TI is the turbulence intensity. The height above ground is given by .1, .2, and .3, meaning 9 m, 12 m, and 17 m, respectively.

Point	N-0°		NE-45°		E-90°		SE-135°		S-180°		SW-225°		W-270°		NW-315°	
	V/VH	TI	V/VH	TI	V/VH	TI	V/VH	TI	V/VH	TI	V/VH	TI	V/VH	TI	V/VH	TI
	[%]	[%]	[%]	[%]	[%]	[%]	[%]	[%]	[%]	[%]	[%]	[%]	[%]	[%]	[%]	[%]
1.1	0.61	23	0.58	19	0.49	24	0.44	29	0.52	25	0.64	20	0.61	22	0.5	28
1.2	0.65	19	0.58	21	0.55	23	0.48	26	0.58	23	0.68	18	0.68	21	0.59	22
1.3	0.72	19	0.62	19	0.60	21	0.52	24	0.66	20	0.75	17	0.70	19	0.64	19
2.1	0.56	23	0.52	24	0.50	26	0.44	30	0.56	25	0.64	19	0.50	26	0.51	26
2.2	0.61	20	0.57	22	0.50	26	0.49	28	0.63	23	0.68	19	0.61	22	0.56	22
2.3	0.63	18	0.64	21	0.57	23	0.54	25	0.71	21	0.72	18	0.66	19	0.59	21
3.1	0.55	26	0.55	22	0.45	27	0.47	28	0.65	22	0.65	21	0.56	23	0.5	24
3.2	0.63	21	0.61	21	0.50	25	0.51	26	0.67	22	0.69	18	0.62	22	0.54	23
3.3	0.64	19	0.65	21	0.58	23	0.61	21	0.70	21	0.72	18	0.62	21	0.58	22
4.1	0.70	21	0.54	25	0.46	27	0.4	31	0.51	25	0.56	22	0.52	26	0.56	24
4.2	0.74	20	0.56	23	0.51	25	0.48	26	0.61	21	0.65	21	0.59	24	0.59	20
4.3	0.77	19	0.62	22	0.55	22	0.53	23	0.65	20	0.67	19	0.66	19	0.67	19

Table 4. Cont.

Point	N-0°		NE-45°		E-90°		SE-135°		S-180°		SW-225°		W-270°		NW-315°	
	V/VH	T.I	V/VH	T.I	V/VH	T.I	V/VH	T.I	V/VH	T.I	V/VH	T.I	V/VH	T.I	V/VH	T.I
	[%]	[%]	[%]	[%]	[%]	[%]	[%]	[%]	[%]	[%]	[%]	[%]	[%]	[%]	[%]	[%]
5.1	0.61	24	0.54	22	0.42	31	0.39	31	0.54	24	0.58	24	0.48	29	0.48	29
5.2	0.70	21	0.61	22	0.46	28	0.48	29	0.63	22	0.61	20	0.59	22	0.54	23
5.3	0.77	19	0.66	23	0.56	25	0.54	26	0.64	20	0.65	20	0.65	20	0.6	21
6.1	0.52	25	0.56	22	0.48	29	0.53	24	0.53	25	0.53	25	0.53	24	0.44	28
6.2	0.60	22	0.61	21	0.58	24	0.55	22	0.55	23	0.59	22	0.58	20	0.52	26
6.3	0.63	19	0.62	21	0.65	20	0.6	20	0.64	21	0.62	21	0.60	20	0.57	22
7.1	0.57	29	0.61	23	0.44	29	0.41	27	0.49	24	0.48	25	0.46	29	0.53	24
7.2	0.70	24	0.63	21	0.52	25	0.47	24	0.54	22	0.57	23	0.55	25	0.63	22
7.3	0.76	19	0.7	20	0.55	24	0.51	23	0.62	20	0.59	21	0.60	22	0.66	20
8.1	0.81	20	0.6	23	0.48	26	0.44	26	0.54	24	0.54	24	0.46	30	0.58	22
8.2	0.85	18	0.69	20	0.47	26	0.47	25	0.53	23	0.56	23	0.51	28	0.66	19
8.3	0.88	16	0.74	20	0.59	23	0.51	24	0.62	21	0.62	21	0.60	22	0.69	18
9.1	0.60	25	0.61	22	0.51	25	0.39	31	0.53	23	0.48	26	0.46	27	0.5	25
9.2	0.62	25	0.63	21	0.57	23	0.48	26	0.59	20	0.55	26	0.52	24	0.56	23
9.3	0.71	20	0.71	19	0.63	22	0.56	24	0.63	19	0.59	23	0.62	22	0.65	20
10.1	0.59	25	0.68	20	0.55	26	0.44	27	0.48	26	0.54	28	0.53	28	0.48	27
10.2	0.66	23	0.7	17	0.62	24	0.5	24	0.56	22	0.56	25	0.62	22	0.52	23
10.3	0.74	21	0.77	18	0.68	21	0.5	24	0.59	21	0.64	21	0.64	19	0.62	21
11.1	0.54	27	0.63	21	0.55	27	0.51	23	0.55	22	0.45	30	0.57	21	0.4	30
11.2	0.58	24	0.7	19	0.66	21	0.54	22	0.61	21	0.51	27	0.63	21	0.5	27
11.3	0.65	21	0.74	19	0.70	20	0.56	21	0.62	19	0.61	23	0.65	20	0.56	22

4.4.2. Wasp Engineering Results

Table 5 illustrates the WASP Engineering results obtained for each direction and for each probe point and level. Since this model used the urban digital terrain model, the results were calculated from the same heights above buildings imposed for wind tunnel results and are presented as deviations (in percentage) according to the following equation:

$$d = \frac{M - WT}{WT} \times 100 \quad (1)$$

where d is the deviation expressed in percentage, WT represents the wind tunnel results (from Table 4) and M the values from the simulated model. In fact, Equation (1) will be used throughout this study to infer the deviation values for the other numerical models used. The absolute deviation ad is computed according to Equation (2) and will be used in the same way hereafter.

$$ad = \left| \frac{M - WT}{WT} \right| \times 100 \quad (2)$$

Table 5 expresses the mean deviation per sector of the wind rose per height. The average is calculated at each height for the 11 points, and Table 6 presents the mean absolute deviation results obtained from WASP Engineering per height and sector.

Figures 17–19 present the graphical form of Table 5, where the mean deviation values (wind and turbulence intensity) are represented for each point and height, respectively.

In terms of mean deviations, it is visible from Figures 17–19 that they diminish with height for both wind and turbulence intensity. It is also clear from Figures 17–19 that WASP Engineering tends to overestimate the wind and underestimate the turbulence intensity and there is a tendency for the deviations for wind and turbulence intensity to be higher for sectors 90°–135° and 270°–225°.

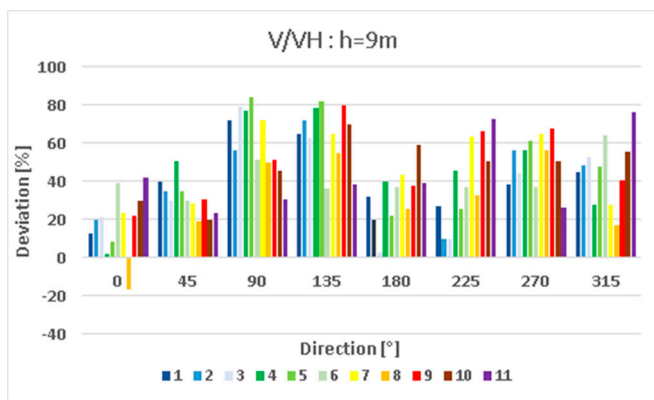
Table 5. Deviation results obtained from the WASP Engineering model. V/VH is the ratio between velocity (V) and velocity at the top of the boundary layer achieved by the model (VH); TI is the turbulence intensity. Values shadowed by dark grey represent deviations with values $\geq 20\%$ or $\leq -20\%$ while values shadowed by light grey color represent deviation values $\geq 10\%$ or $\leq -10\%$ and no shadowed values have deviation values $> -10\%$ or values $< 10\%$. Points denoted by .1 or .2 or .3 mean height above ground at 9 m, 12 m, and 17 m, respectively.

Point	N-0°		NE-45°		E-90°		SE-135°		S-180°		SW-225°		W-270°		NW-315°	
	V/VH	TI	V/VH	TI	V/VH	TI	V/VH	TI	V/VH	TI	V/VH	TI	V/VH	TI	V/VH	TI
	[%]	[%]	[%]	[%]	[%]	[%]	[%]	[%]	[%]	[%]	[%]	[%]	[%]	[%]	[%]	[%]
1.1	12.61	-5.65	39.52	-13.68	71.90	-31.67	64.86	-31.38	32.10	-16.80	26.44	-16.00	37.96	-29.09	44.92	-32.14
1.2	11.60	7.89	43.50	-23.81	57.76	-30.43	59.46	-27.31	25.07	-14.35	22.40	-8.33	27.49	-26.67	29.60	-18.18
1.3	6.09	2.11	37.97	-17.37	48.21	-25.24	54.14	-24.58	15.73	-6.50	14.05	-4.12	27.03	-19.47	25.24	-8.42
2.1	19.51	-0.43	34.47	-15.00	56.31	-28.85	71.50	-34.67	19.51	-12.00	9.25	8.95	56.15	-33.08	47.96	-29.23
2.2	16.77	6.50	30.63	-14.09	63.85	-32.31	61.22	-33.21	13.06	-10.87	9.39	2.11	34.17	-24.09	41.07	-20.00
2.3	19.78	11.11	23.20	-15.24	49.53	-26.52	52.14	-27.60	6.28	-8.10	9.40	2.22	29.02	-14.74	39.24	-19.05
3.1	21.12	-13.08	29.93	-10.45	78.97	-34.44	62.36	-30.71	2.60	1.82	9.82	-5.24	43.68	-27.83	52.46	-25.83
3.2	12.70	0.95	22.82	-10.48	65.69	-30.80	55.35	-27.69	5.97	-5.45	8.58	6.11	33.50	-25.45	46.72	-23.91
3.3	17.43	5.26	20.71	-14.76	46.42	-26.09	34.30	-12.86	7.36	-6.67	8.87	2.22	36.85	-22.38	41.11	-21.82
4.1	1.76	-1.90	50.43	-35.20	76.59	-36.67	78.08	-34.84	39.67	-20.80	45.05	-22.73	56.36	-36.54	27.20	-17.92
4.2	1.25	-2.00	49.59	-31.30	65.31	-33.60	57.37	-26.92	22.82	-10.00	28.88	-20.95	43.02	-32.92	28.03	-7.50
4.3	1.80	-1.58	38.83	-29.09	58.18	-25.91	49.93	-20.87	20.59	-9.50	28.47	-14.21	31.82	-17.37	18.60	-7.37
5.1	8.07	-2.08	34.90	-11.82	84.07	-40.00	81.66	-31.29	22.08	-6.67	25.60	-16.67	60.90	-38.28	47.60	-30.00
5.2	1.43	1.90	26.73	-17.73	75.75	-36.43	55.93	-30.69	12.70	-6.82	26.73	-6.50	37.03	-21.82	38.60	-16.96
5.3	-1.40	4.21	23.54	-25.65	50.55	-31.60	46.30	-27.31	18.63	-5.00	25.33	-11.50	29.70	-17.00	31.67	-14.29
6.1	39.20	-18.80	29.53	-10.91	50.80	-30.34	36.28	-12.08	36.57	-21.60	36.72	-19.60	36.43	-18.33	64.16	-30.00
6.2	26.79	-12.27	24.97	-11.90	32.23	-21.25	39.16	-10.00	38.32	-19.13	29.20	-13.64	32.23	-7.50	47.04	-28.85
6.3	26.37	-2.63	29.03	-16.19	24.38	-10.50	34.23	-6.00	24.40	-15.24	28.91	-13.81	34.74	-12.00	41.16	-19.55
7.1	23.08	-27.93	28.12	-22.61	72.03	-35.17	64.35	-18.89	43.33	-12.08	62.98	-25.60	64.55	-35.86	27.14	-9.17
7.2	5.82	-17.08	28.45	-17.62	52.22	-27.60	53.52	-15.00	37.32	-9.55	42.11	-21.74	44.06	-28.80	14.53	-8.64
7.3	2.63	-0.53	19.56	-16.00	50.07	-27.50	50.53	-16.52	25.81	-5.50	41.98	-16.67	37.56	-21.82	16.32	-6.00
8.1	-16.52	9.50	19.10	-10.87	49.52	-21.15	54.37	-15.77	25.36	-4.58	32.62	-10.83	56.19	-32.33	17.11	-0.91
8.2	-15.11	13.89	8.92	-2.50	59.57	-24.23	53.19	-17.60	36.28	-7.39	34.34	-11.74	47.21	-30.36	9.09	7.89
8.3	-13.02	20.63	6.76	-7.00	33.25	-17.83	49.17	-18.75	23.45	-5.24	27.54	-8.10	31.03	-15.45	10.26	7.22
9.1	21.67	-20.00	30.64	-21.36	50.83	-26.80	79.49	-31.29	37.74	-15.22	66.03	-30.77	67.22	-33.33	40.00	-18.40
9.2	23.70	-24.00	31.14	-20.00	41.43	-23.91	55.13	-23.46	29.99	-7.00	50.21	-33.08	55.03	-27.92	32.97	-16.96
9.3	13.11	-9.50	20.37	-13.68	33.21	-23.64	40.52	-21.67	27.59	-6.32	44.85	-26.52	35.36	-24.09	21.07	-10.00
10.1	29.34	-26.00	19.68	-15.50	45.03	-33.46	69.41	-27.78	58.97	-30.00	50.71	-38.57	50.36	-38.93	55.29	-31.48
10.2	20.63	-22.61	20.11	-2.94	31.64	-28.75	54.15	-20.42	42.17	-20.45	50.14	-32.40	31.64	-22.73	48.08	-21.30
10.3	11.85	-17.62	12.39	-10.00	23.42	-20.00	60.00	-22.92	40.29	-19.05	35.22	-20.48	31.13	-12.11	29.03	-16.19
11.1	41.45	-29.63	23.08	-12.86	30.35	-24.07	38.01	-5.65	38.74	-18.18	72.31	-37.67	25.78	-4.29	76.15	-32.00
11.2	36.47	-23.33	14.51	-6.32	15.15	-8.57	38.75	-7.73	29.63	-16.19	57.01	-32.22	20.51	-9.52	49.85	-29.26
11.3	26.27	-15.24	12.06	-8.95	14.40	-9.00	41.35	-8.57	32.26	-10.00	35.81	-22.61	23.20	-10.00	41.35	-17.73
Ave.	13.76	-6.36	26.82	-15.54	50.26	-26.80	54.43	-21.88	27.04	-11.53	33.24	-15.78	39.66	-23.40	36.38	-17.39
Ave. abs Value	16.56	11.45	26.82	15.54	50.26	26.80	54.43	21.88	27.04	11.64	33.24	17.09	39.66	23.40	36.38	18.31

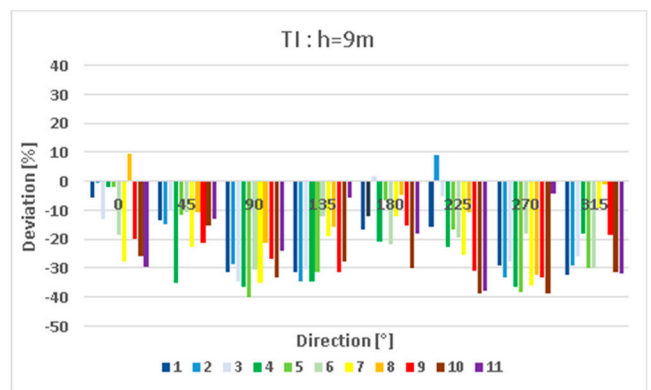
Observing the mean absolute deviations, there is a tendency for the values (both wind speed and turbulence intensity) to be lower when height increases. It is also observed for both wind speed and turbulence values that there are predominant sectors (sectors around 270° and 90°) where the deviations are higher, while for sectors 0° and 180°, the deviations are lower. This may be related to the fact that around 90° and 270° sectors, there are more buildings influencing the passage of the wind flow up to the validation locations when compared with sectors of 0° and 180°, where fewer buildings are present. Overall results obtained by the WASP Engineering tend to be higher than 30% for mean absolute wind speed in all sectors and heights, and higher than 15% for the turbulence intensity equally in all sectors and heights. This means that even using an urban digital terrain model, a non-CFD model such as WASP Engineering can produce reasonable estimates for the wind resource in urban areas.

Table 6. Mean Absolute deviation results obtained from the WASP Engineering model per height and sector. V/VH is the ratio between velocity (V) and velocity at the top of the boundary layer achieved by the model (VH); TI is the turbulence intensity. Values shadowed by dark grey represent deviations with values $\geq 20\%$ or $\leq -20\%$ while values shadowed by light grey color represent deviation values $\geq 10\%$ or $\leq -10\%$ and no shadowed values have deviation values $> -10\%$ or values $< 10\%$. Points denoted by .1 or .2 or .3 mean height above ground at 9 m, 12 m, and 17 m, respectively.

Point	N-0°		NE-45°		E-90°		SE-135°		S-180°		SW-225°		W-270°		NW-315°		Average	
	V/VH	TI	V/VH	TI	V/VH	TI	V/VH	TI	V/VH	TI	V/VH	TI	V/VH	TI	V/VH	TI	V/VH	TI
	[%]	[%]	[%]	[%]	[%]	[%]	[%]	[%]	[%]	[%]	[%]	[%]	[%]	[%]	[%]	[%]	[%]	[%]
.1	21.30	14.09	30.86	16.39	60.58	31.15	63.67	24.94	32.42	14.52	39.78	21.15	50.51	29.81	45.45	23.37	43.07	21.93
.2	15.66	12.04	27.40	14.43	50.96	27.08	53.02	21.82	26.67	11.56	32.64	17.17	36.90	23.43	35.05	18.13	34.79	18.21
.3	12.71	8.22	22.22	15.81	39.24	22.17	46.60	18.88	22.04	8.83	27.31	12.95	31.59	16.95	28.64	13.42	28.79	14.65
Ave.	16.56	11.45	26.82	15.54	50.26	26.80	54.43	21.88	27.04	11.64	33.24	17.09	39.66	23.40	36.38	18.31	35.55	18.26

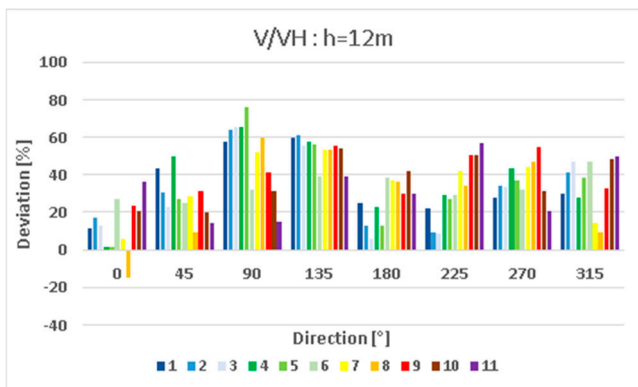


(a)

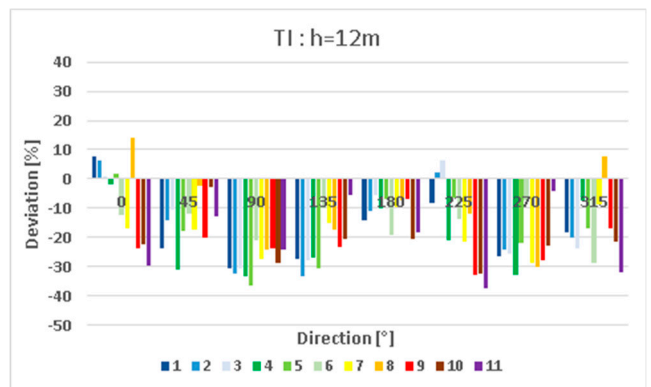


(b)

Figure 17. Mean absolute deviations of the wind (a) and turbulence intensity (b) per direction for the 11 probe validation points at height $h = 9$ m with WASP Engineering.



(a)



(b)

Figure 18. Mean absolute deviations of the wind (a) and turbulence intensity (b) per direction for the 11 probe validation points at height $h = 12$ m with WASP Engineering.

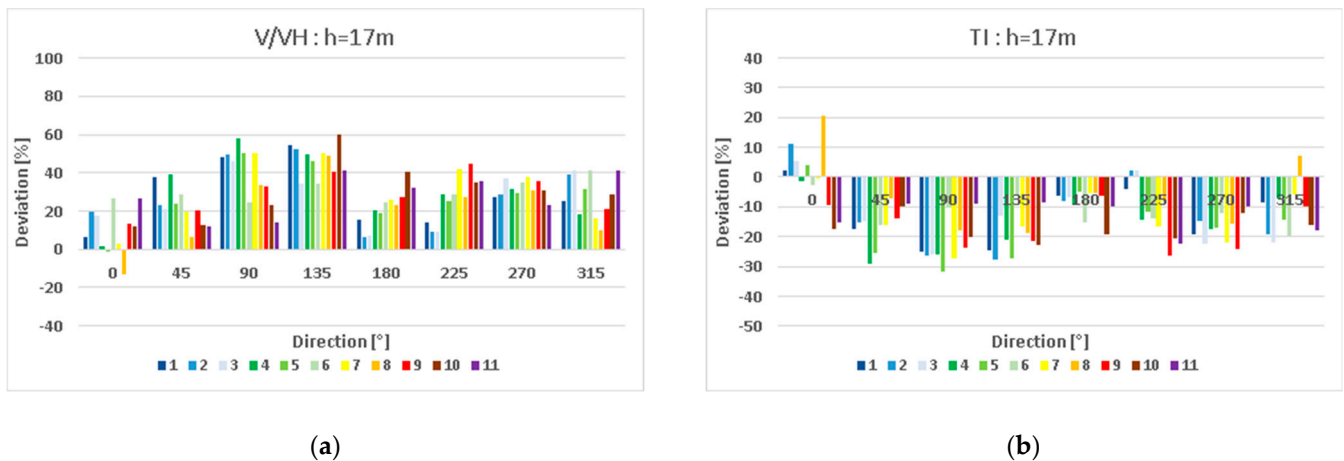


Figure 19. Mean absolute deviations of the wind (a) and turbulence intensity (b) per direction for the 11 probe validation points at height $h = 17$ m with WASP Engineering.

Figure 20 illustrates the mean wind speed patterns for the three heights on the studied sectors of the wind rose (0° , 90° , 180° , and 270°). Model results produce similar patterns for sectors 0° and 180° , and the same happens between sectors 90° and 270° . These spatial results are consistent with the expected results derived from the LINCON simplified flow-turbulence scheme resolved by the WASP Engineering model. In a general way, the spatial wind pattern for all sectors provided by the model does not have the expected wind behavior around obstacles. However, the results here achieved still make this model acceptable to be used as a first approximation for estimating the wind flow in urban environments.

4.4.3. Windsim Results

The WindSim model requires a terrain dataset to produce wind flow estimates. Therefore, using the same urban digital terrain model as the WASP Engineering, it was possible to simulate the wind flow with this CFD model.

Table 7 presents the results obtained with WindSim for each of the eight sectors, each of the 11 points, and heights. The results simulated the same heights above buildings as the wind tunnel experiment.

Table 7. Windsim deviation results. V/VH is the ratio between velocity (V) and velocity at the top of the boundary layer achieved by the model (VH); TI is the turbulence intensity. Values shadowed by dark grey represent deviations with values $\geq 20\%$ or $\leq -20\%$ while values shadowed by light grey color represent deviation values $\geq 10\%$ or $\leq -10\%$ and no shadowed values have deviation values $> -10\%$ or values $< 10\%$. Points denoted by .1 or .2 or .3 mean height above ground at 9 m, 12 m, and 17 m, respectively.

Point	N-0°		NE-45°		E-90°		SE-135°		S-180°		SW-225°		W-270°		NW-315°	
	V/VH	TI	V/VH	TI	V/VH	TI	V/VH	TI	V/VH	TI	V/VH	TI	V/VH	TI	V/VH	TI
	[%]	[%]	[%]	[%]	[%]	[%]	[%]	[%]	[%]	[%]	[%]	[%]	[%]	[%]	[%]	[%]
1.1	0.39	11.40	17.57	35.78	30.93	5.79	9.90	-19.12	-4.47	7.96	1.16	26.71	20.69	10.56	29.53	-9.53
1.2	-1.62	2.50	20.14	-7.55	23.82	-20.24	13.06	-29.33	-5.54	-11.96	0.44	2.95	13.41	-15.54	15.56	-14.42
1.3	-6.16	-13.53	15.59	-14.46	22.28	-29.27	19.51	-33.93	-6.67	-15.45	-2.62	-10.84	16.83	-23.83	13.64	-17.88
2.1	-2.37	19.58	9.75	7.05	6.20	3.42	16.67	-21.90	-5.15	3.40	-7.74	34.92	45.95	-9.18	24.79	-5.62
2.2	-4.22	2.98	7.12	-13.04	17.51	-25.03	15.15	-34.41	-8.60	-3.14	-7.14	1.36	24.95	-20.08	20.15	-16.01
2.3	0.67	-4.69	3.71	-24.46	16.31	-31.27	17.05	-36.64	-10.52	-2.38	-4.72	-10.65	22.04	-23.28	22.26	-26.39
3.1	1.38	6.20	11.48	10.15	40.19	-7.76	16.55	-19.23	-18.36	18.89	-0.91	18.72	34.91	8.76	32.48	7.50
3.2	-5.78	-2.80	5.27	-13.79	32.77	-27.39	16.33	-31.75	-14.27	2.12	-2.27	3.45	25.33	-17.22	28.62	-17.42
3.3	0.24	-11.17	4.75	-28.12	22.05	-35.49	7.20	-26.90	-9.60	-1.64	-0.74	-13.76	29.97	-29.18	27.13	-28.86
4.1	-10.64	26.74	42.95	2.14	41.84	-5.89	28.97	-23.56	19.90	3.64	14.72	15.30	38.92	-4.61	-4.41	14.34
4.2	-12.17	-1.88	39.06	-21.42	35.00	-26.33	19.00	-29.93	5.62	-14.06	3.11	-8.81	29.12	-26.79	1.13	-1.45
4.3	-11.37	-14.55	27.07	-34.28	33.92	-31.68	21.69	-32.33	5.86	-28.81	5.56	-15.06	23.39	-25.96	1.27	-15.97

Table 7. Cont.

Point	N-0°		NE-45°		E-90°		SE-135°		S-180°		SW-225°		W-270°		NW-315°	
	V/VH	T.I	V/VH	T.I	V/VH	T.I	V/VH	T.I	V/VH	T.I	V/VH	T.I	V/VH	T.I	V/VH	T.I
	[%]	[%]	[%]	[%]	[%]	[%]	[%]	[%]	[%]	[%]	[%]	[%]	[%]	[%]	[%]	[%]
5.1	-13.44	15.25	18.66	14.18	50.15	-18.08	31.05	-24.21	2.72	8.10	-4.79	6.38	56.70	-12.62	23.52	-9.01
5.2	-18.78	-1.06	10.78	-16.46	44.12	-32.69	15.86	-35.77	-5.70	-11.70	-2.60	0.41	32.06	-17.14	17.98	-15.00
5.3	-19.15	-8.97	9.45	-34.92	26.08	-37.87	14.11	-37.82	1.04	-19.36	0.00	-13.38	25.40	-26.84	16.00	-23.37
6.1	4.24	6.43	1.76	8.75	4.07	-10.42	-9.95	-2.51	-0.72	6.46	11.09	-0.70	16.28	2.95	13.13	-3.40
6.2	-3.03	-10.64	1.06	-14.81	-4.57	-19.19	-2.30	-16.33	4.07	-11.92	5.46	-15.02	14.73	-9.08	9.17	-23.95
6.3	0.78	-14.92	9.46	-29.26	-3.77	-19.58	2.90	-20.51	-0.93	-18.74	7.55	-25.65	21.83	-25.48	15.95	-26.75
7.1	18.10	-10.57	5.45	11.89	43.69	-13.68	12.24	-11.64	17.21	10.33	34.74	0.30	45.59	-17.78	-10.17	4.20
7.2	-1.17	-21.22	6.90	-9.05	27.17	-25.16	11.22	-21.64	11.59	-10.23	18.19	-23.83	29.17	-31.41	-13.63	-16.27
7.3	-5.71	-18.61	1.97	-20.75	27.27	-34.95	18.86	-29.00	3.26	-17.74	20.28	-34.21	27.46	-36.97	-3.83	-24.02
8.1	-28.45	34.35	-1.88	14.01	27.17	-3.67	20.15	-11.01	-12.26	12.09	7.83	4.17	35.13	-16.70	-12.73	11.63
8.2	-27.20	9.27	-9.33	-2.04	36.34	-27.22	23.49	-27.69	-1.79	-12.54	11.23	-22.25	30.66	-37.13	-14.38	-3.25
8.3	-23.74	1.00	-8.81	-18.20	15.47	-30.69	27.33	-34.95	-6.01	-19.96	9.20	-31.35	21.01	-36.34	-6.72	-14.60
9.1	6.87	7.64	10.98	21.53	19.56	2.30	25.56	-19.89	29.05	16.95	45.17	0.06	48.81	-7.66	8.90	9.03
9.2	8.05	-24.89	11.38	-9.66	13.53	-19.01	13.62	-27.33	18.19	-4.35	30.11	-32.50	39.53	-28.41	7.66	-16.40
9.3	-0.24	-25.23	3.47	-19.38	10.63	-30.17	10.66	-32.91	13.52	-18.54	25.53	-41.00	25.84	-38.47	4.73	-22.74
10.1	-0.51	6.90	-4.24	9.87	10.50	-18.73	24.95	-8.37	26.64	1.64	33.02	-18.38	36.67	-25.64	22.98	-5.76
10.2	-3.84	-17.79	-3.08	0.34	2.98	-28.84	17.67	-19.95	14.45	-11.12	31.60	-31.68	20.66	-29.53	21.85	-18.87
10.3	-5.65	-28.51	-7.18	-18.85	-0.07	-28.29	27.95	-31.42	16.10	-23.19	19.04	-32.37	21.85	-32.35	11.52	-27.23
11.1	10.21	-1.31	0.93	23.93	-3.29	-7.74	11.14	8.47	33.35	18.80	57.55	-14.15	14.32	12.63	28.72	-11.73
11.2	9.46	-21.87	-4.90	-2.07	-12.64	-11.30	12.20	-14.15	20.91	-10.16	41.40	-31.42	8.92	-20.28	16.14	-30.09
11.3	5.83	-28.65	-4.68	-20.71	-9.13	-21.85	17.50	-23.84	19.86	-18.97	20.88	-34.52	12.66	-32.79	19.36	-30.71
Ave.	-4.21	-4.02	7.65	-6.47	19.64	-20.24	15.98	-23.68	4.63	-5.32	12.77	-10.51	27.60	-19.50	11.77	-13.03
Ave. abs Value	8.23	13.12	10.33	16.15	21.67	20.94	16.72	24.19	11.33	12.01	14.80	17.46	27.60	21.61	15.76	15.86

Table 8 presents the results obtained with this model in the same terms as the previously presented models.

Table 8. Mean Absolute deviation results from Windsim per height and sector. V/VH is the ratio between velocity (V) and velocity at the top of the boundary layer achieved by the model (VH); TI is the turbulence intensity. Values shadowed by dark grey represent deviations with values $\geq 20\%$ or $\leq -20\%$ while values shadowed by light grey color represent deviation values $\geq 10\%$ or $\leq -10\%$ and no shadowed values have deviation values $> -10\%$ or values $< 10\%$. Points denoted by .1 or .2 or .3 mean height above ground at 9 m, 12 m, and 17 m, respectively.

Point	N-0°		NE-45°		E-90°		SE-135°		S-180°		SW-225°		W-270°		NW-315°		Average	
	V/VH	T.I	V/VH	T.I	V/VH	T.I	V/VH	T.I	V/VH	T.I	V/VH	T.I	V/VH	T.I	V/VH	T.I	V/VH	T.I
	[%]	[%]	[%]	[%]	[%]	[%]	[%]	[%]	[%]	[%]	[%]	[%]	[%]	[%]	[%]	[%]	[%]	[%]
.1	8.78	13.31	11.42	14.48	25.23	8.86	18.83	15.45	15.44	9.84	19.88	12.71	35.82	11.73	19.21	8.34	19.33	11.84
.2	8.67	10.63	10.82	10.02	22.77	23.85	14.54	26.21	10.07	9.39	13.96	15.79	24.41	22.97	15.11	15.74	15.04	16.82
.3	7.23	15.44	8.74	23.94	17.00	30.10	16.80	30.93	8.49	16.80	10.56	23.89	22.57	30.14	12.95	23.50	13.04	24.34
Ave.	8.23	13.12	10.33	16.15	21.67	20.94	16.72	24.19	11.33	12.01	14.80	17.46	27.60	21.61	15.76	15.86	15.80	17.67

Figures 21–23 depict the values of Table 7, in which the mean deviation values are plotted for wind and turbulence intensity per point and per height, respectively.

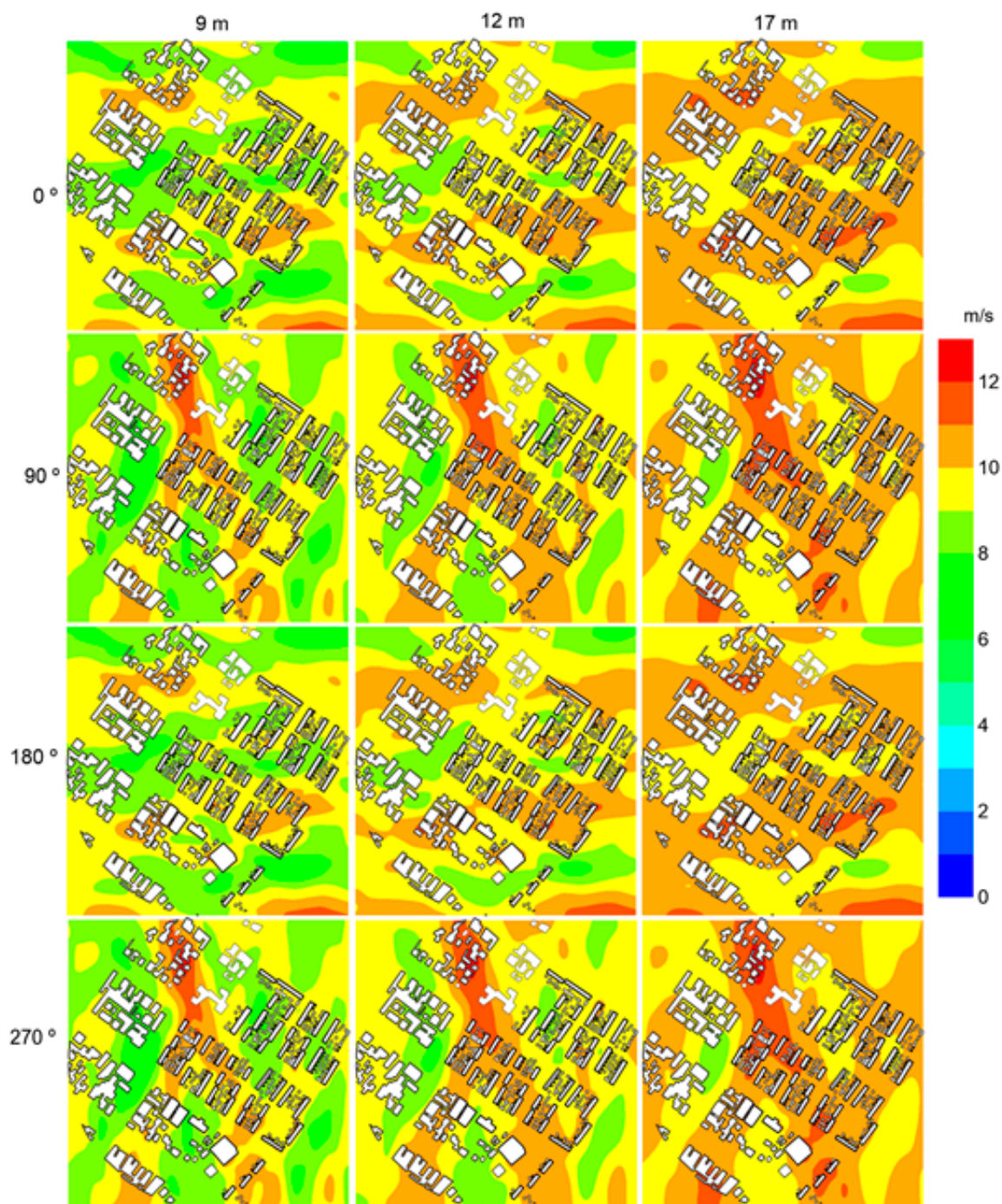


Figure 20. Mean wind speed estimates obtained by the WAsP Engineering model for three heights (9 m, 12 m, and 17 m) and four wind sectors rose (0° , 90° , 180° , and 270°).

In terms of mean deviation values, from Figures 21–23, one observes a different behavior between deviation from velocity and turbulence intensity. While for wind, the mean deviations decrease with height, the turbulence intensity shows the opposite. The WindSim model also tends to overestimate the wind deviations through all points and heights but underestimates the turbulence intensity over all heights except at $h = 9$ m, where there is a tendency to overestimate sectors N and S (0° and 180°).

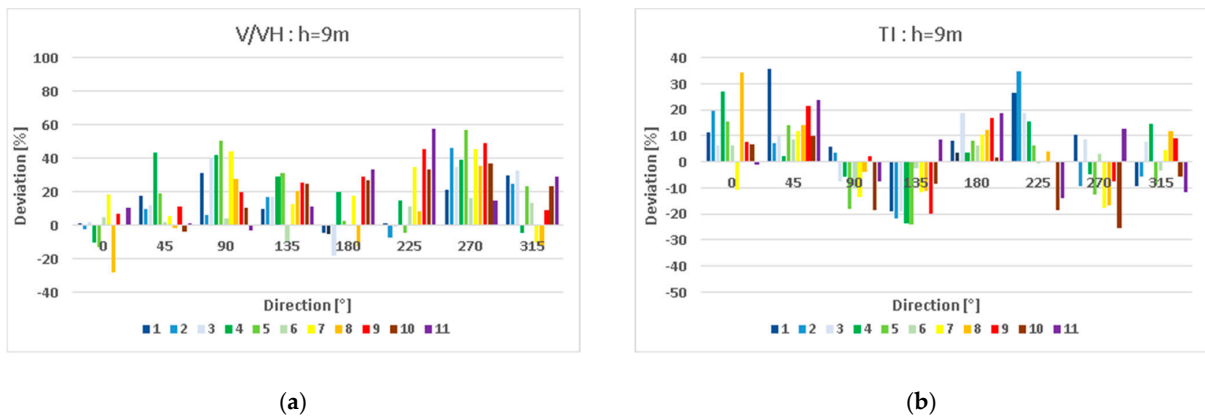


Figure 21. Mean absolute deviations of the wind (a) and turbulence intensity (b) per direction for the 11 probe validation points at height $h = 9$ m with Windsim.

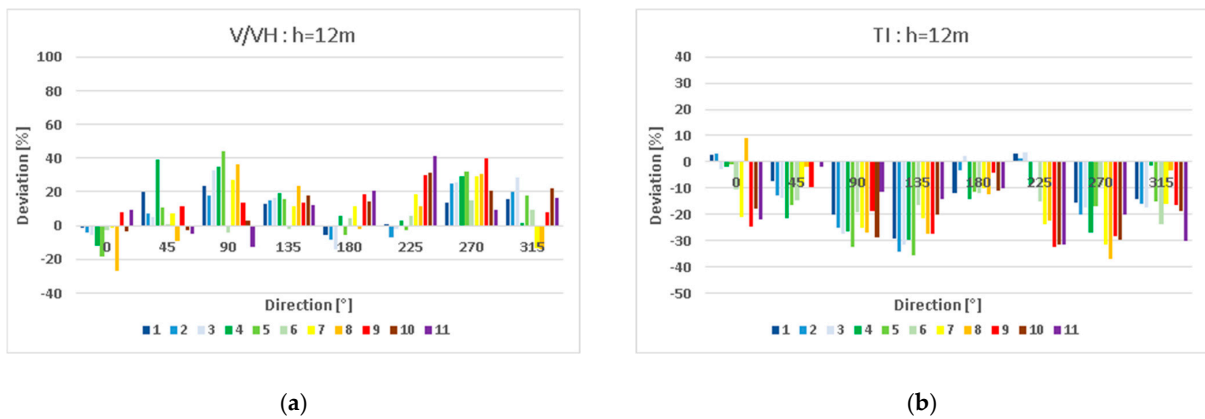


Figure 22. Mean absolute deviations of the wind (a) and turbulence intensity (b) per direction for the 11 probe validation points at height $h = 12$ m with Windsim.

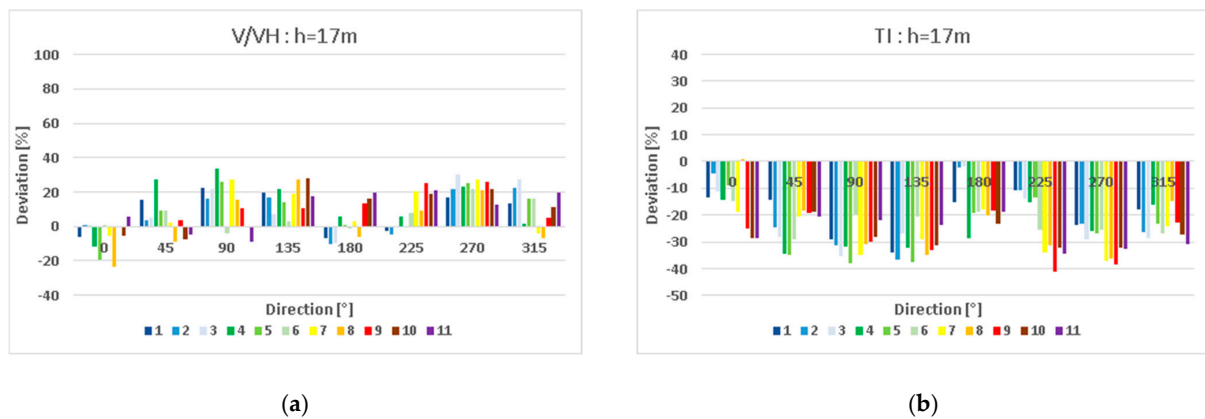


Figure 23. Mean absolute deviations of the wind (a) and turbulence intensity (b) per direction for the 11 probe validation points at height $h = 17$ m with WindSim.

Since WindSim is a CFD model, the obtained results, as expected, are better estimated when compared with WASP Engineering. The overall results show mean absolute deviation values of less than 16% for wind speed through all sectors, while turbulence intensity deviation values are less than 18% for all sectors. The WindSim model has a similar tendency to originate fewer deviations (both wind speed and turbulence intensity) when height grows and shows similar behavior for sectors 270° and 90° and their surroundings

where the deviations are larger, while for sectors 0° and 180° and their surroundings the deviations are lower. Again, this discrepancy may be related to the fact that the wind flow crosses more buildings to the validation points from the sectors 90° and 270° when compared with a smaller number of buildings to cross for 0° and 180° sectors. Globally, the results obtained by the WindSim model are quite good for the urban wind resource assessment, even using an urban digital terrain model with a spatial resolution of $2\text{ m} \times 2\text{ m}$.

Figure 24 illustrates mean speed results for the three heights per four sectors of the wind rose (0° , 90° , 180° , and 270°), where the WindSim model shows a different spatial pattern varying according to angle as expected. The urban digital terrain model produced a concise spatial variability of the wind flow between and around ridges very typical for an urban area which makes this model quite acceptable for urban wind resource assessment.

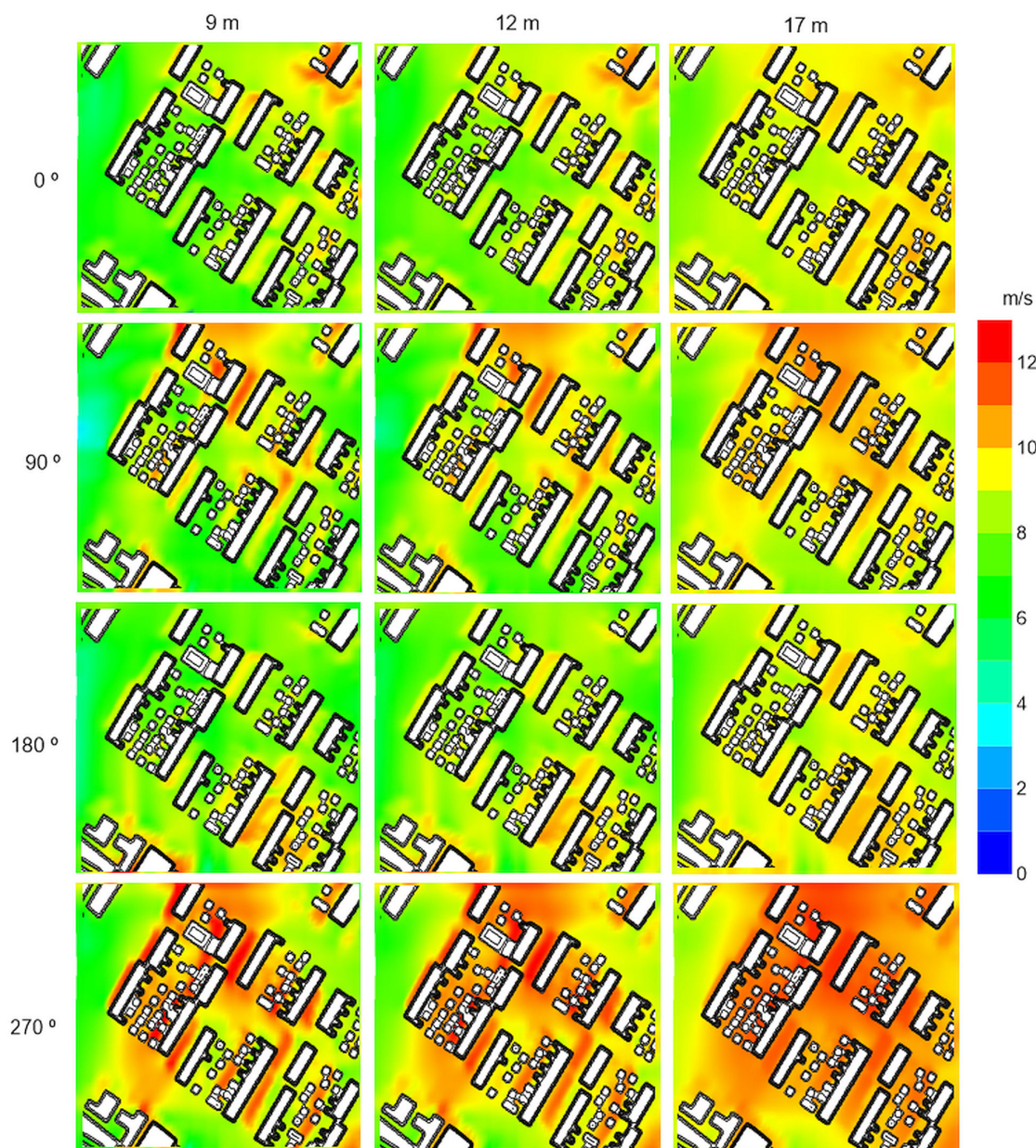


Figure 24. Mean wind speed estimates obtained by the WindSim model for three heights (9 m, 12 m, and 17 m) and four wind sectors rose (0° , 90° , 180° , and 270°).

4.4.4. OpenFOAM Results

Contrary to the previous models, OpenFOAM does not need a terrain dataset to produce wind flow estimates; therefore, only the urban area model was used to provide results.

Table 9 illustrates the results obtained with OpenFOAM for each of the eight sectors, the 11 probe points and heights. The results are simulated for the same heights above buildings as the wind tunnel results. Table 10 presents the mean deviation values according to the results in Table 9.

Table 9. OpenFOAM deviation results. V/VH is the ratio between velocity (V) and velocity at the top of the boundary layer achieved by the model (VH); TI is the turbulence intensity. Values shadowed by dark grey represent deviations with values $\geq 20\%$ or $\leq -20\%$ while values shadowed by light grey color represent deviation values $\geq 10\%$ or $\leq -10\%$ and no shadowed values have deviation values $> -10\%$ or values $< 10\%$. Points denoted by .1 or .2 or .3 mean height above ground at 9 m, 12 m, and 17 m, respectively.

Point	N-0°		NE-45°		E-90°		SE-135°		S-180°		SW-225°		W-270°		NW-315°	
	V/VH	TI	V/VH	TI	V/VH	TI	V/VH	TI	V/VH	TI	V/VH	TI	V/VH	TI	V/VH	TI
	[%]	[%]	[%]	[%]	[%]	[%]	[%]	[%]	[%]	[%]	[%]	[%]	[%]	[%]	[%]	[%]
1.1	14.69	-21.09	9.94	-2.14	16.20	-16.90	10.76	-23.23	3.22	-16.39	0.83	-12.52	-3.13	-10.83	0.52	-3.18
1.2	19.26	-13.58	16.72	-14.14	17.19	-19.40	18.79	-22.44	10.37	-20.07	4.88	-8.23	-1.24	-14.85	12.89	-16.46
1.3	18.23	-20.97	16.44	-8.35	19.33	-18.72	25.77	-25.53	9.61	-16.32	1.87	-3.36	3.61	-9.22	12.18	-6.86
2.1	30.16	-31.10	8.58	-14.22	1.91	-10.90	3.35	-15.56	9.86	-29.85	1.80	-7.78	9.85	-20.55	10.65	-21.03
2.2	29.15	-22.69	17.08	-20.65	22.39	-24.24	19.50	-29.81	6.88	-26.06	5.06	-10.33	8.49	-16.93	20.88	-16.90
2.3	36.20	-18.03	13.43	-19.64	23.83	-24.23	25.77	-33.21	2.77	-20.99	6.10	-6.21	9.04	-6.71	23.14	-16.21
3.1	9.11	-14.41	12.93	-23.28	11.37	-9.31	4.82	-15.37	-15.64	8.78	-4.98	-3.32	8.48	-17.26	25.59	-21.88
3.2	18.78	-15.71	10.98	-20.74	22.68	-22.12	20.52	-32.42	-2.00	-14.38	3.74	-2.47	7.58	-14.15	26.66	-19.60
3.3	32.66	-19.47	12.06	-21.37	21.60	-25.12	12.20	-22.73	4.45	-20.87	5.86	-4.57	15.32	-14.08	24.83	-19.06
4.1	-2.08	-14.82	3.64	-14.54	1.40	0.29	8.64	-11.92	17.47	-17.46	9.02	-12.44	2.81	-22.47	6.73	-23.48
4.2	3.64	-16.20	13.90	-16.59	14.28	-12.88	15.03	-18.51	14.31	-21.73	8.20	-19.58	6.82	-22.73	13.37	-11.07
4.3	10.70	-19.84	14.19	-18.85	26.28	-17.33	22.60	-19.87	14.35	-19.54	13.43	-13.32	7.88	-9.82	8.05	-10.18
5.1	3.13	-17.70	3.59	-9.64	15.59	-18.12	18.22	-18.49	9.68	-19.04	9.85	-25.37	11.19	-25.11	19.65	-32.38
5.2	8.15	-21.17	4.16	-16.00	31.68	-29.45	20.28	-31.74	5.96	-20.19	15.36	-15.06	11.11	-18.92	21.69	-23.63
5.3	10.58	-20.92	7.65	-24.56	24.91	-29.41	23.65	-33.30	13.63	-15.43	16.71	-16.00	11.27	-15.41	20.12	-19.24
6.1	17.23	-6.41	3.07	-14.20	6.07	-24.37	3.81	-20.93	7.85	-16.83	18.63	-23.69	4.82	-10.51	4.93	-5.80
6.2	26.52	-24.72	6.47	-16.91	5.79	-18.70	15.30	-22.53	17.64	-17.29	18.59	-20.15	16.05	-13.98	17.92	-24.02
6.3	35.01	-21.97	15.19	-19.93	8.44	-12.98	14.17	-16.97	12.85	-17.28	21.99	-18.45	21.11	-15.58	25.27	-21.81
7.1	-18.05	-10.44	0.43	-19.27	16.44	-16.83	6.29	3.72	15.89	-12.36	24.80	-20.51	18.19	-28.62	6.30	-16.41
7.2	-9.55	-10.43	6.33	-16.69	18.02	-19.31	13.86	-3.11	22.37	-18.80	18.90	-22.32	16.35	-27.80	5.55	-22.28
7.3	10.82	-18.96	3.07	-14.87	28.28	-25.77	26.99	-16.86	16.90	-15.33	26.73	-19.21	19.70	-24.86	10.06	-17.72
8.1	-20.96	8.16	4.91	-19.73	9.90	-9.60	10.15	-7.32	4.55	-17.46	10.43	-18.40	15.52	-24.03	4.47	-21.85
8.2	-9.33	-9.80	-2.20	-13.55	31.19	-20.76	20.30	-13.95	18.60	-16.45	19.03	-20.85	24.05	-34.61	2.10	-14.36
8.3	-2.94	-6.81	-3.03	-14.14	19.90	-22.30	28.89	-22.73	13.97	-16.10	19.46	-18.62	19.07	-24.76	5.17	-9.23
9.1	-12.93	-0.58	-3.52	-15.77	0.31	-1.34	10.02	-7.19	11.61	-14.61	22.15	-22.31	11.27	-17.03	1.22	-7.13
9.2	7.58	-19.44	5.71	-18.57	7.93	-12.74	18.71	-19.33	14.09	-12.46	22.33	-29.49	23.99	-25.46	12.01	-16.12
9.3	17.14	-22.52	1.97	-12.42	12.23	-19.64	19.02	-25.03	15.88	-11.04	26.69	-25.15	16.21	-24.72	10.68	-16.61
10.1	-27.44	20.19	-5.65	-20.81	-7.88	-3.70	17.99	-17.51	25.47	-27.50	-8.92	1.31	-0.23	-15.05	8.24	-13.50
10.2	-10.11	3.75	-2.96	-3.27	1.31	-15.93	22.79	-21.84	19.95	-18.51	12.91	-13.04	6.04	-20.12	21.14	-20.00
10.3	10.92	-23.71	-5.88	-8.43	5.50	-17.20	35.62	-27.41	23.19	-18.06	16.58	-16.48	13.08	-12.86	15.09	-20.30
11.1	-0.03	-19.11	-6.30	-10.74	-5.25	-14.39	9.94	-18.62	14.07	-12.72	20.76	-16.76	5.75	-11.45	13.49	-15.56
11.2	19.45	-23.77	-5.37	-11.14	-3.21	-12.38	16.40	-20.41	11.98	-14.88	30.12	-27.11	5.37	-16.74	18.01	-23.85
11.3	27.68	-27.37	-2.62	-13.79	2.02	-13.92	21.38	-18.10	17.68	-8.65	22.87	-23.51	10.91	-15.94	26.12	-22.13
Ave.	9.19	-15.20	5.30	-15.42	12.96	-16.96	17.02	-19.70	11.80	-16.85	13.39	-15.62	10.80	-18.28	13.78	-17.27
Ave. abs Value	16.07	17.15	7.58	15.42	13.95	16.98	17.02	19.93	12.87	17.38	14.23	15.69	11.08	18.28	13.78	17.27

Figures 25–27 represent Table 9 values in which the mean deviation values are plotted for wind and turbulence intensity for each point and height, respectively.

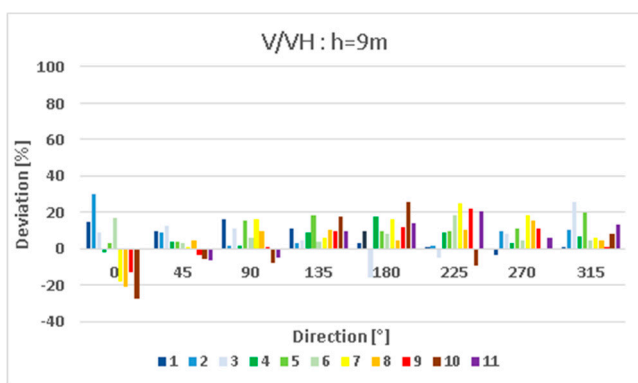
According to Figures 25–27, OpenFOAM tends to overestimate the mean wind deviations as height increases but tends to underestimate the turbulence intensity. With OpenFOAM, there is no clear evidence of sectors having more or fewer deviation values like in WASP Engineering or Windsim results.

In fact, OpenFOAM results are similar when compared with those from the WindSim model. The overall results obtained with OpenFOAM show mean absolute deviation values of less than 14% for wind speed through all sectors, while for turbulence intensity mean deviation value is up to 18%. The obtained results from the wind speed are good for a pure CFD model, and the turbulence intensity results present deviation values slightly lower when compared with Windsim or WASP Engineering results. OpenFOAM presents fewer deviation values (both wind speed and turbulence intensity) in points at a lower height. Sector 45° has the lowest mean deviations, and the other sectors present a similar range of mean deviations. The fact that the wind flow crosses more buildings to reach the validation points on sectors 90° and 270° is not affecting the results from OpenFOAM.

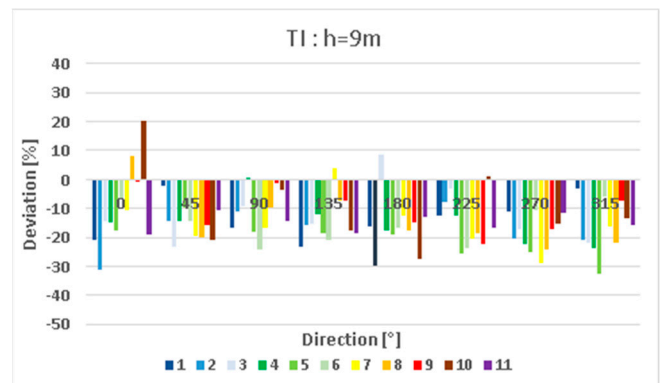
Figure 28 illustrates the mean wind speed results for the three heights (0°, 90°, 180°, and 270°). OpenFOAM shows an expected spatial variability of the wind flow in an urban area. The wake effect is better resolved for the obstacle influence in the 3D structure of the wind. Regardless of the problem with the turbulence intensity values, this CFD model is the most adequate and reliable tool for assessing wind resources in an urban area.

Table 10. Mean Absolute deviation results from OpenFOAM per height and sector. V/VH is the ratio between velocity (V) and velocity at the top of the boundary layer achieved by the model (VH); TI is the turbulence intensity. Values shadowed by dark grey represent deviations with values $\geq 20\%$ or $\leq -20\%$ while values shadowed by light grey color represent deviation values $\geq 10\%$ or $\leq -10\%$ and no shadowed values have deviation values $> -10\%$ or values $< 10\%$. Points denoted by .1 or .2 or .3 mean height above ground at 9 m, 12 m, and 17 m, respectively.

Point	N-0°		NE-45°		E-90°		SE-135°		S-180°		SW-225°		W-270°		NW-315°		Average	
	V/VH	TI	V/VH	TI	V/VH	TI	V/VH	TI	V/VH	TI	V/VH	TI	V/VH	TI	V/VH	TI	V/VH	TI
	[%]	[%]	[%]	[%]	[%]	[%]	[%]	[%]	[%]	[%]	[%]	[%]	[%]	[%]	[%]	[%]	[%]	[%]
.1	14.17	14.91	5.69	14.94	8.39	11.43	9.45	14.53	12.30	17.55	12.01	14.95	8.29	18.45	9.25	16.56	9.95	15.41
.2	14.68	16.48	8.35	15.30	15.97	18.90	18.32	21.46	13.10	18.26	14.47	17.15	11.55	20.57	15.66	18.93	14.01	18.38
.3	19.35	20.05	8.68	16.03	17.48	20.60	23.28	23.80	13.21	16.33	16.21	14.9	13.38	15.81	16.43	16.31	16.00	17.99
Ave.	16.07	17.15	7.58	15.42	13.95	16.98	17.02	19.93	12.87	17.38	14.23	15.96	11.08	18.28	13.78	17.27	13.32	17.26



(a)



(b)

Figure 25. Mean absolute deviations of the wind (a) and turbulence intensity (b) per direction for the 11 probe validation points at height $h = 9$ m with OpenFOAM.

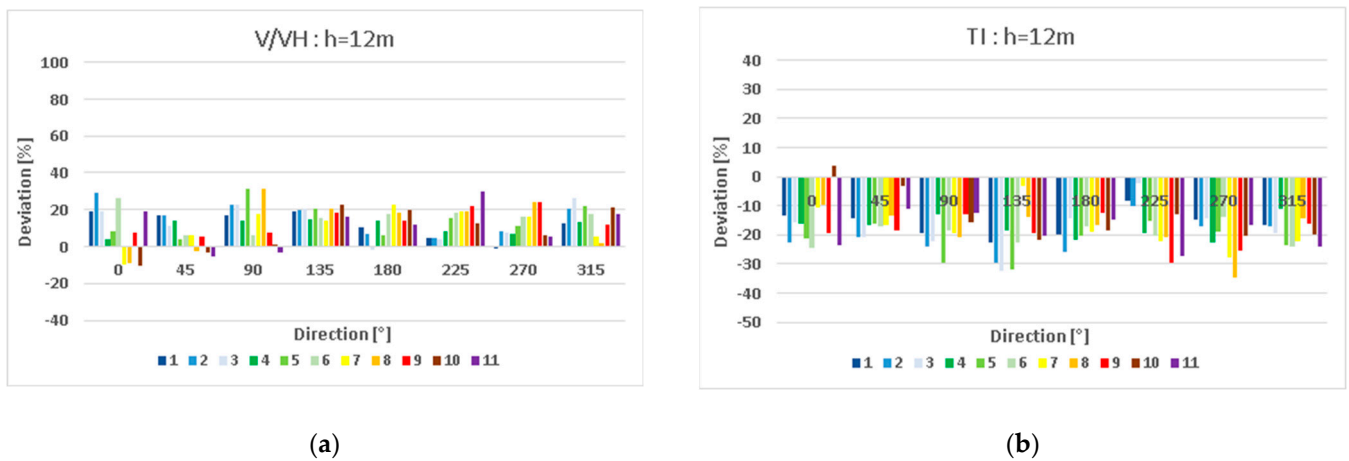


Figure 26. Mean absolute deviations of the wind (a) and turbulence intensity (b) per direction for the 11 probe validation points at height h = 12 m with OpenFOAM.

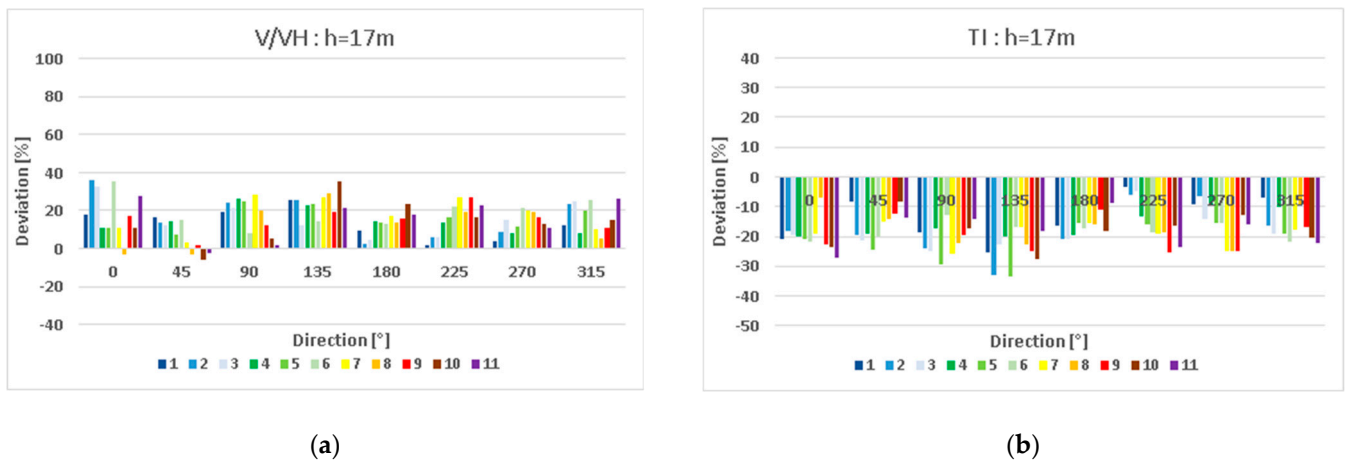


Figure 27. Mean absolute deviations of the wind (a) and turbulence intensity (b) per direction for the 11 probe validation points at height h = 17 m with OpenFOAM.

4.4.5. Overall Results

In this section, the overall results obtained for the three selected models are presented (Table 11). The results are the mean deviation and the mean absolute deviation for all points in all sectors and all heights.

Table 11. Overall results obtained from models, WAsP Engineering (non-CFD), Windsim (CFD) and OpenFOAM (CFD). V/VH is the ratio between velocity (V) and velocity at the top of the boundary layer achieved by the model (VH); TI is the turbulence intensity.

Model	Average		Average Absolute Values	
	V/VH	TI	V/VH	TI
	[%]	[%]	[%]	[%]
Wasp Engineering	35.20	−17.33	35.55	18.26
Windsim	11.98	−12.85	15.80	17.67
OpenFOAM	11.49	−16.91	13.32	17.26

In terms of average deviation values, all models tend to overestimate the wind flow and underestimate the turbulence intensity. As expected, WAsP Engineering tends to overestimate the results more than Windsim and OpenFOAM. The obtained values are consistent with the recent publication involving numerical studies as appointed in Section 1. In terms of turbulence intensity, the values obtained are satisfactory, especially since this is not a CFD model and the accuracy for urban environments is lower. Moreover, the fact that WAsP Engineering and WindSim do not use a 3D mesh based on urban fabric, and instead use an urban digital terrain model may influence the results.

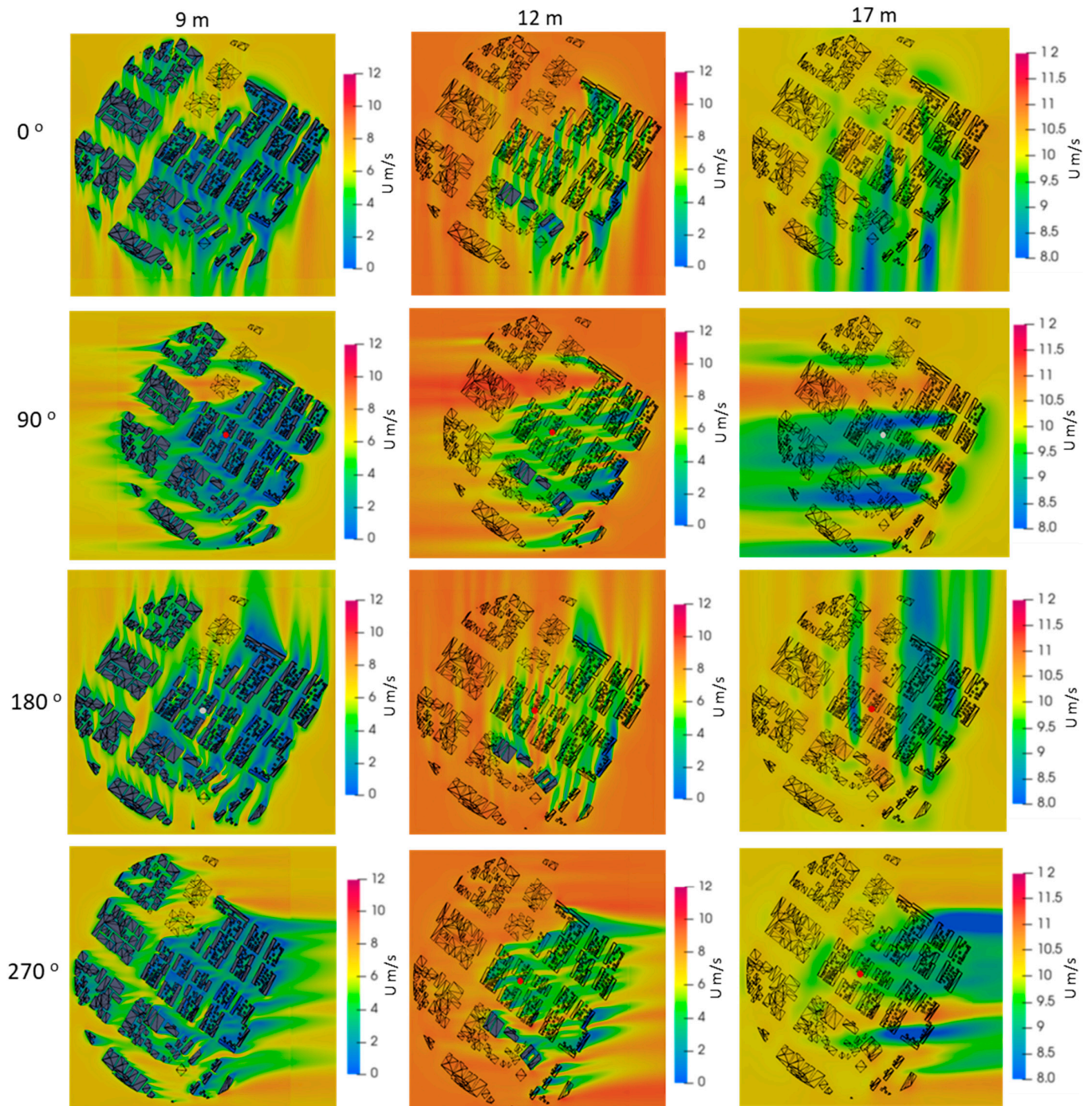


Figure 28. Mean wind speed estimates obtained by the OpenFOAM CFD model for three heights (9 m, 12 m, and 17 m) and four wind sectors rose (0°, 90°, 180°, and 270°).

Figures 29 and 30 depict, respectively, the mean wind and mean turbulence deviation roses obtained for the 11 test points per height and per model. It is visible that in terms of wind speed deviations, all models tend to show higher deviations for sectors 90°, 135°, and 270°, both for wind speed and turbulence intensity. The same pattern is visible when height varies. However, it is visible that the deviation values decrease when the height increases, which is expected since the influence of the buildings on the wind flow diminishes as height increases. In a general way, it is clearly visible that both CFD models (OpenFOAM and WindSim) produce lower mean wind speed deviations when compared with the WASP Engineering.

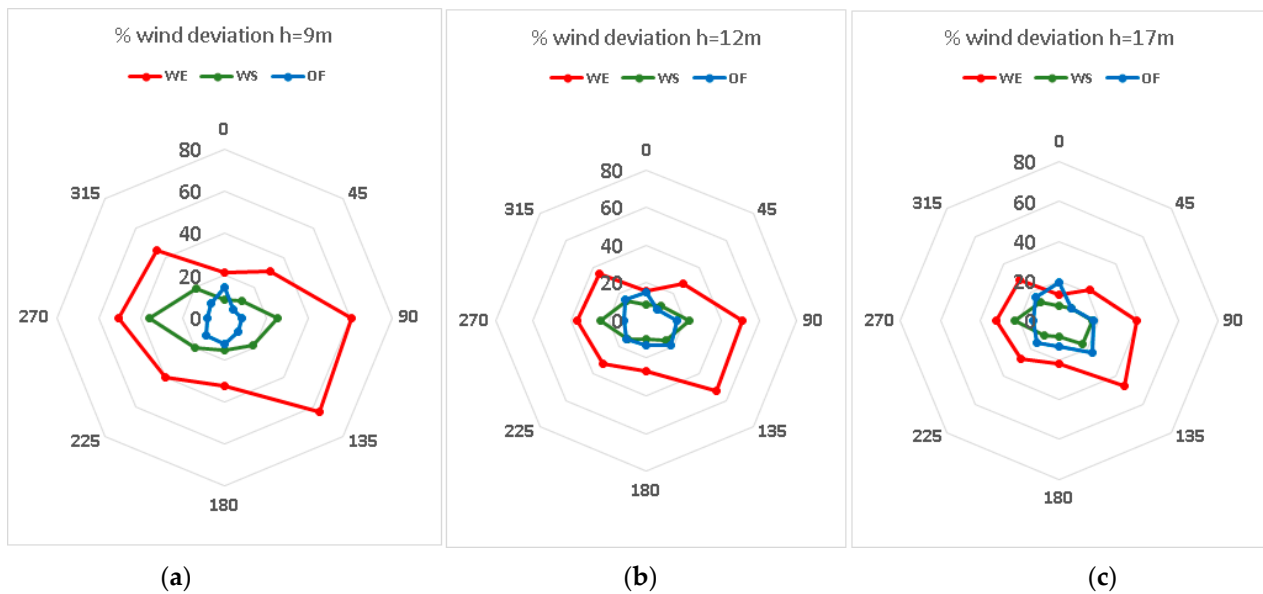


Figure 29. Overall mean wind speed absolute deviation per points 1, 2, 3 and per height (a)—9 m, (b)—12 m, and (c)—17 m above ground.

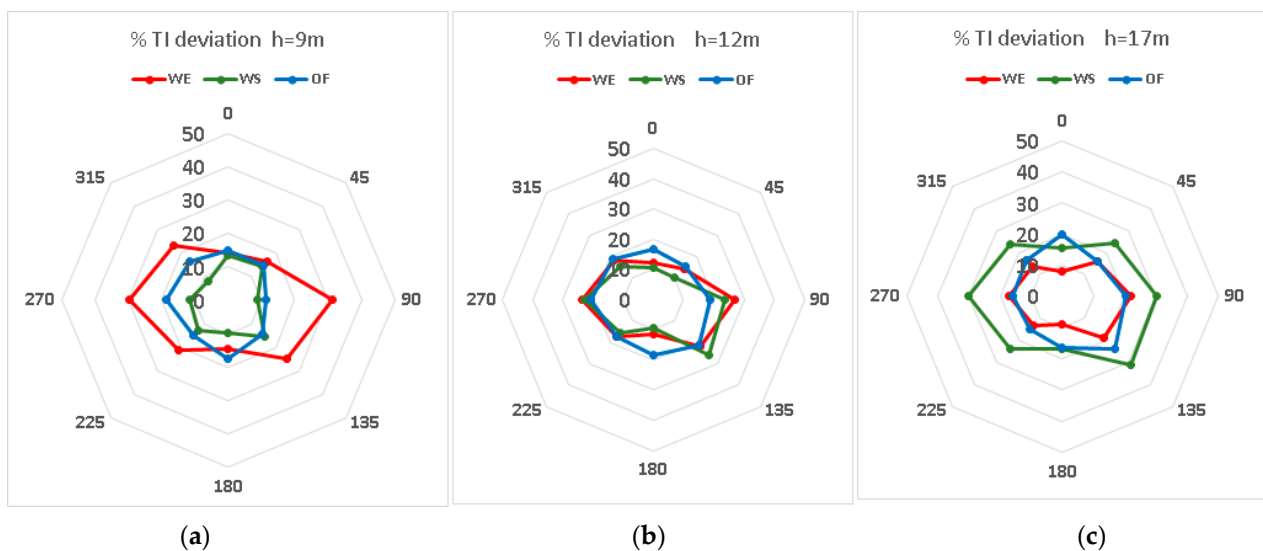


Figure 30. Overall mean turbulence intensity absolute deviation per points 1, 2, 3 and per height (a)—9 m, (b)—12 m, and (c)—17 m above ground.

4.5. Discussion

Results achieved by the models are satisfactory for wind speed and turbulence intensity. Both CFD models, WindSim and OpenFOAM, produce mean wind speed deviation between 14% and 16%, while WAsP Engineering presents deviations in wind speed up to 35%. Although the deviation values may seem high, one should consider that the urban area under analysis is quite dense and characterized by narrow streets and irregular building heights, which constitutes a challenge in wind behavior modeling, especially in large urban areas.

The WindSim model shows lower deviation at low levels near the ground, where the turbulence is stronger, but the deviation values increase with height where the turbulence was imposed. Contrarily, WAsP Engineering showed lower deviations with increasing heights. In the case of OpenFOAM, the deviations are similar for all heights.

The overall results showed that the building density in the urban area is of major importance when there is the need to simulate the wind flow, and it must be considered in both types of models—CFD or Non-CFD models. The higher building density and the most irregular heights occur in the sectors aligned with 90° and 270° sectors. In this sense, and based on the results, it is possible to observe that the less accurate estimates occurred in these sectors, as expected.

5. Conclusions and Perspectives

Three models were used and presented in this paper to study the wind flow over an urban area and validated with wind tunnel results for different sectors of the wind rose. A non-CFD-Model WAsP Engineering—a world-leading commercial software to solve the wind flow for wind farm resource assessment is used against two CFD models. One commercial is the WindSim model—which is commonly used to solve the wind flow over very complex terrain to produce wind farm estimates—and the freeware OpenFOAM model, a pure CFD model adequate to solve transient or stationary case studies for many different engineering areas.

The numerical model's performance was evaluated with data from physical modeling developed in a wind tunnel. A zone in a sub-urban region was modeled. A wind flow for a sub-urban exposure area was modeled, resulting in a roughness length of 0.87 m and a turbulence intensity of 18% at 60 m high.

The three numerical models were run with the same sub-urban wind profile characterized by the mean wind profile and the turbulence intensity profile. A deviation parameter was defined to evaluate the performance, and it was applied to evaluate the mean wind speed and the turbulence intensity faced in wind tunnel results.

The CFD models—OpenFOAM and WindSim—produced the best mean wind speed estimates. The mean deviation for the mean speed was 14% and 16%; respectively, while applying the WAsP Engineering model, the mean deviation was 36%. In WindSim and WAsP Engineering model, deviations are more pronounced for directions 90° and 270° and less pronounced for 0° and 180°. Although these deviations are high, it should be noted that this type of urban area (densely distributed) is still a challenge for wind behavior modeling since it is composed of very narrow streets and irregular height buildings and the probe points were strategically chosen at the most challenging zones where strong convergence or divergence wind flows are expected to occur.

The WindSim and OpenFOAM models achieved a turbulence intensity mean absolute deviation near 18% like the one obtained with WAsP Engineering, although, while in WAsP Engineering, the lowest deviation values increase with height, where the turbulence intensity parameter is imposed, both CFD models showed the opposite trend, i.e., the mean absolute turbulence intensity deviations increase with height.

The wind speed and turbulent intensity deviation roses, at all heights, show the pattern already identified according to whose sectors have more pronounced deviations, and it was verified higher deviation values for 90° and 270° sectors and lower deviation values for 0° and 180° sectors. An exception to this occurred for the WindSim model at the

lowest height. This exception is probably due to the automatic smoothing effect imposed on those sectors due to their higher complexity and irregularity (this model performs a gentle smoothing of the terrain in high complexity situations to avoid non-convergence criteria for each simulated direction) to improve convergence.

In the first approach, it is concluded that all the models presented here can produce reliable results for planning purposes—identifying promising sites for urban wind exploitation. However, the CFD models are more reliable and capable of inferring the wind flow with more detail and, consequently, more suitable to study detailed sheltering obstacle effects on wind flow, turbulence or other phenomena, whereas models such as OpenFOAM, or similar, should be used.

In summary, from the results presented here, it can be concluded that for planning purposes in the scope of smart and sustainable cities, models such as WindSim would be suitable to give a reasonable estimate of the wind flow over areas within urbanized regions, such as cities or groups of neighborhoods ideal for the installation of small wind turbines. OpenFOAM would be an excellent choice to describe the detailed wind flow for more detailed studies where 3D wind characterization is needed. Nevertheless, the simulated results can be even more improved with OpenFOAM when applying different turbulence model parameterizations to study the deviation values of wind speed and turbulence intensity which was not covered in this study mainly due to limitations of WASP Engineering and WindSim, which would not enable us to compare the results in all three models.

Author Contributions: Conceptualization, C.A., C.J. and S.T.; methodology, all authors; data processing, C.P., G.D. and M.L.; software, C.P., G.D. and M.L.; validation, C.P., G.D. and M.L. writing—original draft preparation, S.T., C.J. and C.P.; writing—review and editing, all authors. All authors have read and agreed to the published version of the manuscript.

Funding: This research received external funding from the REGEDIS network within the Programa Iberoamericano de Ciencia y Tecnología para el Desarrollo, from the Brazilian ANEEL R&D project IBITU.INTELIPREV, funding and fellowships, and from the ANII (Innovation and Research National Agency of Uruguay) with the project FSE_1_2011_1_6674 “Eólica Urbana”.

Institutional Review Board Statement: This study did not perform research on humans or animals.

Informed Consent Statement: Not applicable.

Acknowledgments: The authors would also like to thank their institutions for the internal support of the research presented here.

Conflicts of Interest: The authors declare no conflict of interest. The funders had no role in the design of the study; in the collection, analyses, or interpretation of data; in the writing of the manuscript, or in the decision to publish the results.

References

1. Ishugah, T.F.; Li, Y.; Wang, R.Z.; Kiplagat, J.K. Advances in Wind Energy Resource Exploitation in Urban Environment: A Review. *Renew. Sustain. Energy Rev.* **2014**, *37*, 613–626. [\[CrossRef\]](#)
2. Karthikeya, B.R.; Negi, P.S.; Srikanth, N. Wind Resource Assessment for Urban Renewable Energy Application in Singapore. *Renew Energy* **2016**, *87*, 403–414. [\[CrossRef\]](#)
3. Simões, T.; Estanqueiro, A. A New Methodology for Urban Wind Resource Assessment. *Renew Energy* **2016**, *89*, 598–605. [\[CrossRef\]](#)
4. Bentham, T.; Britter, R. Spatially Averaged Flow within Obstacle Arrays. *Atmos. Environ.* **2003**, *37*, 2037–2043. [\[CrossRef\]](#)
5. Syngellakis, K.; Clement, P.; Cace, J. Wind Energy Integration in the Urban Environment-WINEUR. 2005. Available online: http://www.urbanwind.net/pdf/Reports_country_description.pdf (accessed on 27 July 2022).
6. Toja-Silva, F.; Kono, T.; Peralta, C.; Lopez-Garcia, O.; Chen, J. A Review of Computational Fluid Dynamics (CFD) Simulations of the Wind Flow around Buildings for Urban Wind Energy Exploitation. *J. Wind Eng. Ind. Aerodyn.* **2018**, *180*, 66–87. [\[CrossRef\]](#)
7. Walker, S.L. Building Mounted Wind Turbines and Their Suitability for the Urban Scale—A Review of Methods of Estimating Urban Wind Resource. *Energy Build.* **2011**, *43*, 1852–1862. [\[CrossRef\]](#)
8. Yang, A.S.; Su, Y.M.; Wen, C.Y.; Juan, Y.H.; Wang, W.S.; Cheng, C.H. Estimation of Wind Power Generation in Dense Urban Area. *Appl. Energy* **2016**, *171*, 213–230. [\[CrossRef\]](#)

9. Liu, S.; Pan, W.; Zhao, X.; Zhang, H.; Cheng, X.; Long, Z.; Chen, Q. Influence of Surrounding Buildings on Wind Flow around a Building Predicted by CFD Simulations. *Build. Environ.* **2018**, *140*, 1–10. [[CrossRef](#)]
10. Plate, E.J. *Engineering Meteorology: Fundamentals of Meteorology and Their Application to Problems in Environmental and Civil Engineering*; Elsevier Scientific Publishing Company: Amsterdam, The Netherlands, 1982; p. 740. [[CrossRef](#)]
11. Mertens, S. Wind Energy in Urban Areas: Concentrator Effects for Wind Turbines Close to Buildings. *Refocus* **2002**, *3*, 22–24. [[CrossRef](#)]
12. Micallef, D.; van Bussel, G. A Review of Urban Wind Energy Research: Aerodynamics and Other Challenges. *Energy* **2018**, *11*, 2204. [[CrossRef](#)]
13. Baklanov, A.; Grimmond, C.S.B.; Mahura, A.; Athanassiadou, M. *Meteorological and Air Quality Models for Urban Areas*; Springer: Berlin/Heidelberg, Germany, 2009; pp. 1–183. [[CrossRef](#)]
14. Lane, S.E.; Barlow, J.F.; Wood, C.R. An Assessment of a Three-Beam Doppler Lidar Wind Profiling Method for Use in Urban Areas. *J. Wind Eng. Ind. Aerodyn.* **2013**, *119*, 53–59. [[CrossRef](#)]
15. Wang, Q.; Wang, J.; Hou, Y.; Yuan, R.; Luo, K.; Fan, J. Micrositing of Roof Mounting Wind Turbine in Urban Environment: CFD Simulations and Lidar Measurements. *Renew. Energy* **2018**, *115*, 1118–1133. [[CrossRef](#)]
16. Stathopoulos, T.; Alrawashdeh, H.; Al-Quraan, A.; Blocken, B.; Dilimulati, A.; Paraschivoiu, M.; Pilay, P. Urban Wind Energy: Some Views on Potential and Challenges. *J. Wind Eng. Ind. Aerodyn.* **2018**, *179*, 146–157. [[CrossRef](#)]
17. Tasneem, Z.; al Noman, A.; Das, S.K.; Saha, D.K.; Islam, M.R.; Ali, M.F.; R Badal, M.F.; Ahamed, M.H.; Moyeen, S.I.; Alam, F. An Analytical Review on the Evaluation of Wind Resource and Wind Turbine for Urban Application: Prospect and Challenges. *Dev. Built Environ.* **2020**, *4*, 100033. [[CrossRef](#)]
18. Miao, Y.; Liu, S.; Chen, B.; Zhang, B.; Wang, S.; Li, S. Simulating Urban Flow and Dispersion in Beijing by Coupling a CFD Model with the WRF Model. *Adv. Atmos. Sci.* **2013**, *30*, 1663–1678. [[CrossRef](#)]
19. Piroozmand, P.; Mussetti, G.; Allegrini, J.; Mohammadi, M.H.; Akrami, E.; Carmeliet, J. Coupled CFD Framework with Mesoscale Urban Climate Model: Application to Microscale Urban Flows with Weak Synoptic Forcing. *J. Wind Eng. Ind. Aerodyn.* **2020**, *197*, 104059. [[CrossRef](#)]
20. Rakai, A.; Kristóf, G. CFD Simulation of Flow over a Mock Urban Setting. In Proceeding of the 5th OpenFOAM Workshop, Gothenburg, Sweden, 21–24 June 2010; pp. 2–5.
21. Kadaverugu, R.; Purohit, V.; Matli, C.; Biniwale, R. Improving Accuracy in Simulation of Urban Wind Flows by Dynamic Downscaling WRF with OpenFOAM. *Urban Clim.* **2021**, *38*, 100912. [[CrossRef](#)]
22. Stull, R.B. *An Introduction to Boundary Layer Meteorology*; Springer: Berlin/Heidelberg, Germany, 1988. [[CrossRef](#)]
23. Arya, S.P. *Air Pollution Meteorology and Dispersion*; Arya, S.P., Ed.; Oxford University Press: New York, NY, USA, 1999; Volume 310.
24. Simiu, E.; Scanlan, R.H. *Wind Effects on Structures: An Introduction to Wind Engineering*; Wiley: Hoboken, NJ, USA, 1986; p. 589.
25. Holmes, J.D. *Wind Loading of Structures*, 1st ed.; Taylor & Francis: New York, NY, USA, 2001; Volume 1, ISBN 0-203-30164-1.
26. American Society of Civil Engineers. *Minimum Design Loads and Associated Criteria for Buildings and Other Structures*; American Society of Civil Engineers: Reston, VA, USA, 2017; ISBN 9780784414248.
27. *EUROCODE Designers' Guide to EN 1991-1-4 Eurocode 1: Actions on Structures, General Actions Part 1–4*; European Committee for Standardization: Brussels, Belgium, 2007.
28. Simiu, E.S.R.H. *Wind Effects on Structures: Fundamentals and Applications to Design*; John Wiley: New York, NY, USA, 1996.
29. Hussain, M.; Lee, B.E. A Wind Tunnel Study of the Mean Pressure Forces Acting on Large Groups of Low-Rise Buildings. *J. Wind Eng. Ind. Aerodyn.* **1980**, *6*, 207–225. [[CrossRef](#)]
30. Grimmond, C.S.B.; Oke, T.R. Aerodynamic Properties of Urban Areas Derived from Analysis of Surface Form. *J. Appl. Meteorol.* **1999**, *38*, 1262–1292. [[CrossRef](#)]
31. Carl, P. Type, Field, Culture, Praxis. *Archit. Des.* **2011**, *81*, 39–45. [[CrossRef](#)]
32. Astrup, P.; Larsen, S.E.; Rathmann, O.; Madsen, P.H. WAsP Engineering—Wind Flow Modelling Over Land and Sea. *Wind Eng.* **1999**, *7*, 179–184.
33. Wallbank, T. WindSim Validation Study: CFD Validation in Complex Terrain. *CFD Valid. Complex Terrain* **2008**.
34. Weller, H.G.; Tabor, G.; Jasak, H.; Fureby, C. A Tensorial Approach to Computational Continuum Mechanics Using Object-Oriented Techniques. *Comput. Phys.* **1998**, *12*, 620. [[CrossRef](#)]
35. Standen, N.M. *A Spire Array for Generating Thick Turbulent Shear Stress for Natural Wind Simulation in Wind Tunnels*; AIVC: Ottawa, ON, Canada, 1972.
36. Irwin, H.P.A.H. The Design of Spires for Wind Simulation. *J. Wind Eng. Ind. Aerodyn.* **1981**, *7*, 361–366. [[CrossRef](#)]
37. Cermak, J.E.; Davenport, A.G.; Durgin, F.H.; Irwin, P.A.; Isyumov, N.; Peterka, J.A.; Ramsay, S.R.; Stathopoulos, T.; Steckley, A.C.; Tieleman, H.; et al. *Wind Tunnel Studies of Buildings and Structures*; American Society of Civil Engineers: Reston, VA, USA, 1999; Volume 1.
38. Ferry, M. New Features of MIGAL Solver. In Proceedings of the 9th International Phoenix User Conference, Moscow, Russia, 2002; pp. 23–27.

39. Mirza, S.; Niwalkar, A.; Anjum, S.; Bherwani, H.; Singh, A.; Kumar, R. Studying Impact of Infrastructure Development on Urban Microclimate: Integrated Multiparameter Analysis Using OpenFOAM. *Energy Nexus* **2022**, *6*, 100060. [[CrossRef](#)]
40. Jiang, Y.; Przekwas, A. Implicit, Pressure-Based Incompressible Navier-Stokes Equations Solver for Unstructured Meshes. In Proceedings of the 32nd Aerospace Sciences Meeting and Exhibit, Reno, NV, USA, 10–13 January 1994. [[CrossRef](#)]
41. Petersen, E.L.; Mortensen, N.G.; Landberg, L. Wind Resources Part II: Computational Methods. In Proceedings of the 1993 European Community Wind Energy Conference, Lübeck-Travemünde, Germany, 8–12 March 1993; pp. 611–614.
42. Farr, T.G.; Rosen, P.A.; Caro, E.; Crippen, R.; Duren, R.; Hensley, S.; Kobrick, M.; Paller, M.; Rodriguez, E.; Roth, L.; et al. The Shuttle Radar Topography Mission. *Rev. Geophys.* **2007**, *45*, RG2004. [[CrossRef](#)]